SPIN TRANSPORT MEASUREMENTS IN $GaAs$ QUANTUM DOTS

A DISSERTATION
SUBMITTED TO THE DEPARTMENT OF PHYSICS
AND THE COMMITTEE ON GRADUATE STUDIES
OF STANFORD UNIVERSITY
IN PARTIAL FULFILLMENT OF THE REQUIREMENTS
FOR THE DEGREE OF
DOCTOR OF PHILOSOPHY

Joshua A. Folk
March 2003

I certify that I have read this dissertation and that in my opinion it is fully adequate, in scope and quality, as a dissertation for the degree of Doctor of Philosophy.

Charles M. Marcus
(Principal Advisor)

I certify that I have read this dissertation and that in my opinion it is fully adequate, in scope and quality, as a dissertation for the degree of Doctor of Philosophy.

David Goldhaber-Gordon

I certify that I have read this dissertation and that in my opinion it is fully adequate, in scope and quality, as a dissertation for the degree of Doctor of Philosophy.

Katheryn A. Moler

Approved for the University Committee on Graduate Studies.

Abstract

This thesis explores the spin dynamics of lateral quantum dots in $GaAs/AlGaAs$ heterostructures, including the first demonstration of a geometry capable of measuring mesoscopic spin currents. The term "quantum dot" as used in this thesis refers to partially-confined regions connected to two leads by quantum point contacts. Because the quantum dots investigated in these experiments are gate-tunable, they are used to probe the range from open systems (dot conductance $g > e^2/h$) to confined electron systems (dot conductance $g < e^2/h$).

In open dots, there is at least one fully transmitting channel of conductance in both the entrance and exit point contacts, and transport is characterized by conductance fluctuations. These fluctuations are analogous to the universal conductance fluctuations (UCF) observed in disordered systems, and reflect the quantum interference of transport paths through the device. In Chapter 2 we explore the degree to which the spin physics of such systems is reflected in their conductance, and shows non-trivial effects such as spin-orbit interaction or broken spin degeneracy.

Even a simple picture of the spin physics in open dots, however, would predict that at large in-plane fields the transport through such a device would consist of spin-polarized electrons. This is explored in Chapter 3: here we present, for the first time, a direct measurement of the spin currents emitted from open quantum dots (and other mesoscopic structures) at high field. We find that the transport behavior of open dots is indeed consistent with a simple picture of the two spin species, separated by a Zeeman energy, undergoing uncorrelated spin-resolved conductance fluctuations and therefore leading to fluctuations in the spin polarization of emitted current.

Finally, in Chapter 4, the measurement of quantum dot spin states is extended into the Coulomb blockade regime. Energy spectroscopy measurements of quantum dot ground and excited states show clear signatures of ground state spin transitions as consecutive electrons

are added, although clearly these measurements are inconsistent with a system that is spin degenerate at low field. Surprisingly, when the spin polarization of electrons emitted during transport is measured directly, there appears to be no correlation between the emitted current polarization and the ground state spin transitions measured at the same time.

Acknowledgements

I begin this Acknowledgements section with my reading committee: Katheryn Moler, David Goldhaber-Gordon, and Charlie Marcus. Kam was a valuable mentor when I was a teaching assistant for her class, but more than that she has always put a human, friendly, face on the crazy life of being a young professor. David has been for me both a friend, and also an inspiration for his marvelous combination of kindness and humility, experimental creativity, general inquisitiveness, and razor-sharp instincts in physics. I thank them both for providing role models, both personal and professional, for a career in physics.

The person most directly responsible for my ability to complete this PhD thesis work successfully was my advisor, Charlie Marcus. I started working for Charlie when I was still an undergrad, before I had much experience in experimental physics at all. I really have Charlie to thank for my training up to now, both as an experimentalist and as a contributing member of the physics community. It was from him I learned the finer art of silver soldering, and how to make measurements with a lock-in amplifier. Even more, it was from him that I began to pick up the instincts of a successful experimentalist: which avenues to attack first when confronted with a problem, when to abandon the path you're on and try another, and when to keep digging because the path you're on will, eventually, lead to success.

Charlie has always been active in pursuing his own (wide-ranging) friendships in the wider community of mesoscopic physicists, theorists and experimentalists alike, and always welcomed us, his students, to join in. This has left me in the best position a PhD student could hope for, as he finishes his degree and heads out on his own, of having an open line of communication to an entire community of experts. Even more valuable, I learned from Charlie's easy social interactions with others in our area to have the self-confidence to talk to experts in the new fields where I am headed, and to interact with them as collegues.

Finally, as the writing of this thesis has taken a few months and I have begun work

on a new project as a post-doc, I am discovering now the number of ways that Charlie made the academic research process easy for his students. Although cutting-edge research in a complex new field is never really an easy prospect, I am beginning to realize all the administrative hurdles Charlie removed from our paths so that we could focus on science. Life is a grad student can be frustrating at times, with conflicting demands on our time and the growing pains of coming to maturity in a scientific community. During my last few years I focused too much on those frustrations, without understanding that in many ways my scientific life as a grad student was as easy as it would every be again.

A large fraction of my life over the last four years has been spent in Charlie's lab. Starting from the very beginning, I worked with the older grad students Andy Huibers, Sam Patel, and Duncan Stewart, and in the course of learning new equipment and new physics together we became close friends. I have to thank Sam, Andy, and Duncan for an additional, more technical, contribution to my PhD work: not only did they graduate having brought the lab equipmnent to a very high level of performance, they also left me with an arsenal of devices—reflecting more than a year of cleanroom suffering—that would continue to fuel my research for the next two years.

It was in Charlie's lab, while still an undergrad, that I met Sara Cronenwett. During the four years of my PhD she became one of the most important people in my life; together we fought through research frustrations, and kept each other sane when other aspects of life seemed just to be closing in from all sides. Sometimes that sanity took the form of 3 A. M. runs from the Stanford physics building, and at other times took the form of more trips to the Sierras than any one grad student career should by rights be allowed to contain. Dominik Zumbuhl entered Charlie's lab at nearly the same time as me, and over the last four years has grown for me from simply a friend to an extremely valuable resource for physics and experimental questions and discussions.

When the lab moved to Harvard, two years ago, I was introduced to a crop of new students. All of them—Jeff, Ron, Alex, Andrew and Heather—I have to thank for making the move just about as painless as I could have hoped for. It took less than 4 months after the move for equipment to be in place and ready for the first series of measurements. Andrew has since become a valued hiking, movies, dinner, and carpentry companion. In addition, he and I spent a year in 2000-2001 attempting to study optical polarization of nuclii in $GaAs$, a frustrating project in which both of us learned a lot about what to do (and not to do) when an experiment doesn't work. I wish him the best of luck in life, and

success in whatever ventures he pursues in the future.

Ron and I started to work together immediately after he joined our group. Initially, we worked together with Alex on spin measurements using quantum dots fabricated in the arms of an Aharanov-Bohm ring. These were devices from Leo Kouwenhoven's group at Delft; I was grateful to have the opportunity to measure them. Soon, however, Ron and I chose a slightly different direction, which ultimately led to the spin polarization measurements presented in this thesis. In all of those experiments, Ron and I worked as partners and I thank him for his apparently limitless optimism and energy, his unwillingness to be defeated by a stubborn sample. In addition, it was Ron who fabricated the devices used for those measurements, and I regret that I only once brought him orange juice and doughnuts during his many midnight e-beam sessions.

I thank those not in my lab, especially Myles and Eric, for providing the the friendship outside of work without which a grad student would probably go insane. I thank my sister and brothers, Anna, Peter, and Kenyon, for always being supportive. And most important, I thank my parents for sympathizing with me, encouraging me, mainaining an interest in my research, and ultimately for having instilled in me as I was growing up the desire to inquire and to understand that has brought me to the point where I find myself today.

Contents

List of Figures

Chapter 1

Experimental Techniques and Apparatus

1.1 Introduction

This thesis describes measurements of the spin physics of electrostatic-gate-defined quantum dots in the two-dimensional electron gas (2DEG) of a $GaAs/AlGaAs$ heterostructure. In a basic picture, this kind of quantum dot can be thought of simply as a confined region of electrons, connected to the bulk by an entrance and an exit lead. All measurements were done at low temperature (below 500 mK) for two reasons. First, spin physics is typically probed by looking at the two spins split by a Zeeman energy, which is greater than thermal broadening only at these low temperatures. Second, several of the experiments combined coherent orbital quantum dot behavior with spin physics, and the orbital coherence time in these systems is strongly suppressed at higher temperatures. Because the measurements combined both orbital and spin physics, it was also important to have both fine control over a small (< 250 mT) perpendicular magnetic field as well as the capability of applying a large (up to 9 T) in-plane magnetic fields. These experimental details will be described in this chapter. For more complete general descriptions of the system, see Ref. [3].

1.2 Low Temperature Measurement

The experiments were all performed in ^3He refrigerators or $^3He/^4He$ dilution refrigerators, with base temperatures of 300 mK or 30 mK respectively. One of the most difficult technical parts of low temperature transport measurements is ensuring that the temperature of the electrons engaged in transport is as low as, or close to, the base temperature of the refrigerator. We used low-temperature electrical filters to achieve this, and monitored our electron temperature using Coulomb blockade peak width, which is a direct measure of the thermal broadening of the Fermi sea in these devices. Temperatures reported in this thesis are in all cases *electron* temperature, rather than the lattice temperature or the mixing chamber temperature of the refrigerator.

1.3 In-plane/Perpendicular Field Apparatus

One technology developed for this thesis work was the combination of a small field coil providing a field perpendicular to the mounted sample, together with a standard high-field cryogenic solenoid providing fields in the plane of the heterostructure. The function of the perpendicular field coil was to allow fine control over these fields, which strongly affect the orbital physics of the device. The primary solenoid provided the large fields necessary for Zeeman splitting, oriented parallel to the plane of the heterostructure samples so as not to strongly influence the orbital behavior of the system (see Fig. 1.1).

The cryogenic (liquid helium) solenoids commonly used for producing multi-tesla fields for mesoscopic experimental work have 2 or 3 *in* bores, into which the ^3He or dilution refrigerators are inserted. In all cases, our samples were mounted with the axis of the solenoid approximately in the plane of the heterostructure. Error in this alignment was generally less than one degree, controlled by fine-threaded screws on the mounting hardware for the sample. One technique which was tried, and rejected, was to put the superconducting coil of the perpendicular field magnet *inside* the inner vacuum can (IVC) of the refrigerator, but this attempt failed because, without liquid helium to cool the magnet wires, quenches were frequent and catastrophic (wires burnt). Another disadvantage of this approach was that without metal shielding between the magnet coil and the sample, a considerable amount of electrical noise was coupled into the sample and low temperatures were not attained (electron temperature $T_e > 150$ mK in a dilution refrigerator with base temperature 30 mK).

To solve both of these problems, a different architecture was designed in which the

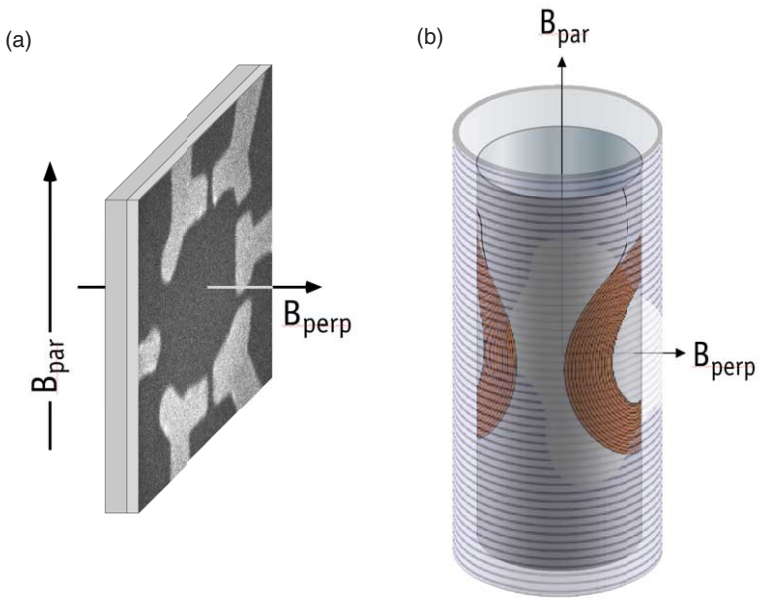

Figure 1.1: (a) Schematic indicating orientation of B_{par} and B_{perp} with respect to the planar quantum dot. (b) Illustration showing placement of superconducting coils used to generate B_{perp} relative to the vacuum can and the primary solenoid used to produce B_{par}. (The orientation of B_{par} within the plane is not accurately depicted but was in a few cases investigated.)

perpendicular field coils (roughly 400 turns) were mounted (using GE varnish and dental floss) to the outer wall of the IVC. For this a new IVC had to be built, with a slightly narrower section inserted into the bore of the primary solenoid to allow space for both the field coils and the IVC inside the primary solenoid. This design worked well, and provided the fields (up to $\sim 250mT$) needed for experiments presented in sections 2.2, 3.2, and 4.2. The disadvantage of this technique was that the considerable torques generated when both perpendicular and in-plane fields were large caused the (slightly flexible) refrigerator structures to bend temporarily (elastically in most cases), and created a misalignment of the sample with the in-plane field that depended on the torque applied.

The final magnet design we tried, in order to address this last problem, was to mount the perpendicular field coils on a metal (brass) structure that was fixed to the primary solenoid. This structure had a clear bore of 1.7 *in*, and the IVC built to work with this system had an external diameter of 1.5 *in* in the segment which was inserted into the magnet. This design was used only for the experiments reported in sections 3.3 and 4.4, and its degree of effectiveness has not yet been fully determined. One disadvantage of this design is that the perpendicular field that can be developed is in general weaker than in the previous design,

as there is less room for perpendicular field coils (due to an additional metal layer).

Both of these designs suffer from one common problem: there appears to be slight ($< 5\ mT$) hysterysis in the field at the sample location as a function of applied current. We believe that this was due to flux trapping in the superconducting wire used for the perpendicular field coils.

1.4 *GaAs/AlGaAs* Heterostructures

For all of the work presented in this thesis, the heterostructures were chosen for special properties related to each particular experiment. Detailed descriptions of the three heterostructures that we used are given below.

The experiments presented in Chapters 2 and 4.2 (Dots A, B, and C in Fig. 1.2) were performed on a 2DEG (2385A) grown by Cem Duruöz in the group of Jim Harris at Stanford University. While its mobility ($\sim 140,000$) was unremarkable as far as *GaAs/AlGaAs* heterostructures are concerned, the unique feature of this 2DEG was its "quietness," or stability from charge-noise. This was critical for these experiments, because the experiment in Chapter 4 measured Coulomb blockade peak position (essentially a measure of ground state energy, whether electrostatic, orbital, or spin-related), and the other two experiments relied on the conductance of dot point contacts staying fixed over the course of several data taking runs (many hours). Although the origin of charge-noise is poorly understood in these systems, empirically one can say that the electrostatic environment seen by structures (for example quantum dots) in a typical 2DEG fluctuates in discrete "switching" events on a timescale ranging from fractions of a second (considered a "bad" device) to hours or even days (considered a "good" device). All devices fabricated on this 2DEG showed similar freedom from charge-noise, with switching events occuring on a timescale of days or longer. The growth parameters for this 2DEG are described below:

$GaAs$ substrate
$300nm$ $GaAs$ buffer
100 period superlattice of $3nm$ $GaAs/10nm$ $AlGaAs$
$50nm$ $AlGaAs$
$1000nm$ $GaAs$
$40nm$ $Al_{0.34}Ga_{0.66}As$
$40nm$ $Al_{0.34}Ga_{0.66}As$ with Si modulation-doping $1 \times 10^{18} cm^{-3}$
$10nm$ $GaAs$

A similarly quiet heterostructure was used for the few-electron dot labelled Dot D. This was grown by Micah Hansen in the group of Art Gossard at UCSB, and has the parameters given below:

$GaAs$ substrate
$50nm$ $GaAs$ buffer
30 period superlattice of $3nm$ $GaAs/3nm$ $AlGaAs$
$800nm$ $GaAs$
$40nm$ $Al_{0.3}Ga_{0.7}As$
Si δ-doping $4 \times 10^{12} cm^{-2}$
$60nm$ $Al_{0.34}Ga_{0.66}As$

The experiments presented in Chapter 3 and 4.5 (Dot E) were performed on a 2DEG grown by Vladimir Umansky at the Weizmann Institute. For this heterostructure, the "quietness" was more typical, but its distinguishing feature was its extremely high mobility (lack of scatterering centers). A high mobility was critical for these experiments because they were based on a measurement of the current injected ballistically from a point contact "emitter" (of order 20 nm wide) into a bulk ("base") 2DEG region, and collected (ballistic trajectories only) into a second point contact after a path length of several microns. The presence of *any* scattering events during the trajectory between emitter and collector would lead to the current being lost (draining to the grounded reservoir in the base region rather than impinging on the collector), and furthermore would complicate the focusing action of the small perpendicular field that directs electron trajectories from the emitter to collector regions. Using this heterostructure, we were able to achieve coupling efficiencies as high as $\sim$

30% (30% of the current from the emitter was coupled ballistically through several microns into the $\sim 20\ nm$ opening of the collector), making the measurement considerably easier and the experiment less confusing to interpret. The growth parameters of the Umansky 2DEG are given below:

$GaAs$ substrate
30 period superlattice of $GaAs/AlGaAs$
$1200nm\ GaAs$
$68nm\ Al_{0.36}Ga_{0.64}As$
$Si\ \delta$-doping $2.5 \times 10^{12} cm^{-2}$
$26nm\ Al_{0.36}Ga_{0.64}As$
$8nm\ GaAs$

1.5 Quantum Dots

Again, I refer interested readers to Ref. [3] for further explanations, but very briefly a quantum dot is—for the purposes of this thesis—defined as an area of electrons confined by electrostatic depletion gates, with entrance and exit leads to 2DEG reservoirs. The entrance and exit leads are quantum point contacts (QPC's) passing anywhere between one partially transmitting mode and a few fully transmitting modes. The dots measured for this work are shown in Fig. 1.2.

1.6 Basic Mesoscopic Phenomena

1.6.1 Conductance Fluctuations

At the low temperatures ($< 100mK$) used for many of the experiments described in this thesis, electron coherence lengths greatly exceed the dot dimensions. The point contacts that serve as entrance and exit leads for the dots inject electrons with a spread of trajectories, and in the semi-classical approximation transport through the dot is determined by taking a coherent sum of the different paths that an electron may take, bouncing off the walls of the dot, from the entrance to the exit. Because this coherent sum is strongly sensitive to the exact shape of the dot (in addition, of course, to the Fermi wavelength and

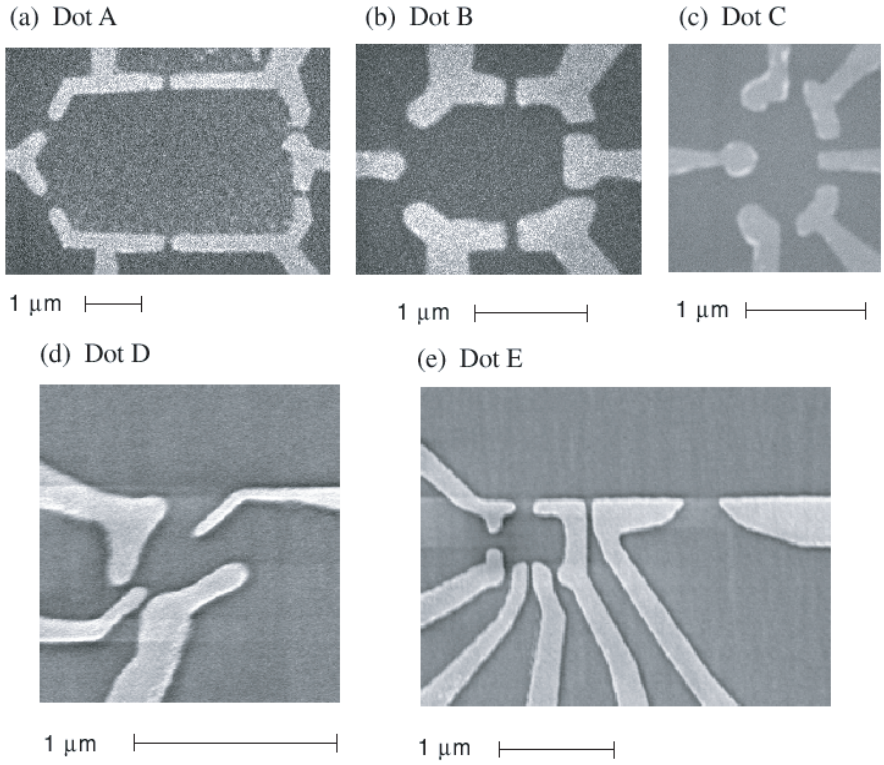

Figure 1.2: SEM micrographs of dots similar to those measured for experiments presented in this thesis. (a) 8 μm^2, (b) 1 μm^2, and (c) 0.25 μm^2 dots fabricated on CEM2385A. (d) few-electron dot based on a design in Ref. [56] and fabricated on 010219B. (e) 0.1 μm^2 dot built into the focusing geometry described in Chapter 3.

therefore to the Fermi velocity of the electron), the conductance of the dot shows random but repeatable flucuations as a function of dot shape—controllable using an electrostatic voltage on a nearby gate—that are akin to Universal Conductance Fluctuations (UCF) observed in disordered systems. A more complete presentation of conductance fluctuations may be found in Ref. [3].

1.6.2 Coulomb Blockade

When the point contacts of a quantum dot are set to pass less than one fully transmitting mode, electrons are required to tunnel onto and off of the device, and transport through the device is characterized by Coulomb blockade. Coulomb blockade refers to the fact the conduction through the dot is prevented for most settings of the electrostatic gates of the dot, because the available energy levels in the dot are not aligned with the Fermi energy in

the leads. Because of this misalignment, an electron is unable to tunnel *onto* the dot if the energy needed to add an additional electron (from N to $N+1$ electrons) is above the Fermi energy in the leads, and an electron is unable to tunnel *off* of the dot if the extra energy carried by that electron (as the dot returns to N electrons) is less than the Fermi energy in the leads. When this tunnelling (both onto and off of the dot) is energetically allowed, however, a sharp peak in conduction is observed which is known as a Coulomb blackade peak.

The energy needed for the additional $(N+1)$ electron to tunnel onto the dot can be written as the difference in ground state energy U for the dot before the electron has arrived, $U(N)$, and after the electron has tunnelled on, $U(N+1)$. The full description of the energy on an N electron dot is given in Ref. [2]:

$$H = \sum_i \varepsilon_i + E_c N^2 - JS(S+1) + Sg\mu B. \tag{1.1}$$

There are several terms in the energy difference $\Delta U = U(N+1) - U(N)$, including as the largest contribution the "charging energy" $N^2 E_c = N^2 e^2/C_{dot}$, which is simply the additional Coulomb energy needed to add the $N+1$'th electron to a confined area. (C_{dot} is the self-capacitance of the dot.) In addition, there is an orbital quantum energy, ε_{N+1}, associated with the eigenenergy of the $N+1$'th electron wavefunction. Most relevant for this thesis, however, there is also a Zeeman energy associated with the change in spin as the $N+1$'th electron is added. In particular, the quantity $U(N+1) - U(N)$ includes the term $(S_{N+1} - S_N)g\mu B$, where g is the bare g-factor in $GaAs$ and S is the spin on the dot.

The energy difference ΔU can be probed by looking at the change in the voltage V_g that must be applied to an electrostatic side gate in order to bring the N and N+1 electron ground state energies into degeneracy (and thereby allow transport, creating a Coulomb blockade peak). In particular, one finds $eC_{gate}V_g/C_{dot} = \Delta U + \mu$, where μ is the chemical potential of the dot. The derivation of this equation is shown in Ref. [4]. In the absence of other effects, this leaves $eC_{gate}V_g/C_{dot} \sim (S_{N+1} - S_N)g\mu B$, and therefore the position in gate voltage, V_g, of the Coulomb blockade peak will depend in a simple way on both the applied magnetic field and the spin transition. In many cases it is experimentally easier to look at Coulomb blockade peak *spacing*, ΔV_g, rather than position, and we find

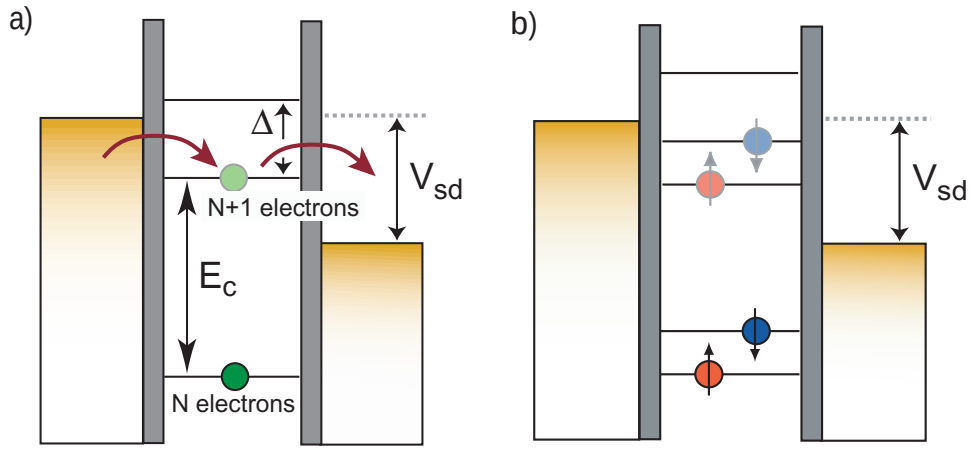

Figure 1.3: A schematic showing how a finite source-drain bias may be used to examine excited orbital states (a) as well as excited spin states (b). A peak in differential conductance dI/dV is observed whenever an excited state of the N+1 electron system passes the source (higher voltage, on the left), or when an excited stae of the N electron system passes the drain.

$$eC_{gate}\Delta V_{gate}/C_{dot} \sim (S_{N+2} + S_N - 2 \times S_{N+1})g\mu B \tag{1.2}$$

When a finite dc source-drain bias voltage, V_{sd}, is applied to the dot, transport may also occur through excited state levels as long as both the excited state and the ground state of the N+1 electron system fall within the bias window, see Fig. 1.3. Thus a finite source-drain may be used to probe excited states of both the N and N+1 electron systems, as described more thoroughly in Ref. [5]. In section 4.4 we describe how this technique has been applied to look, in particular, at excited spin states.

1.6.3 Transverse Electron Focusing

The experiments reported in chaper 3 of this thesis rely on a technique developed a decade ago known as transverse electron focusing [6]. This technique has been used previously to study phenomena ranging from anisotropy in the band structure of metals [7, 8] and semiconductors [9, 10] to composite fermions in the fractional quantum Hall regime [11]. In transverse electron focusing, the trajectories of electrons from an emitter QPC are bent 180° by a perpendicular magnetic field to fall on a collector QPC a few microns away. The condition for the perpendicular field to bend electron trajectories into the collector, spaced

a distance d away, is that d must be an integral multiple of the cyclotron diameter, $d = 2Nm^*v_F/eB_\perp$, where m^* is the effective electron mass, v_F the Fermi velocity, and N is any integer (this assumes specular scattering from a flat wall separating emitter and collector). When N is greater than one, this assumes specular scattering of electron trajectories from the wall in between the point contacts.

There are two primary advantages of transverse electron focusing, over a more straightforward geometry in which no perpendicular field is applied and the straight-path trajectories from the emitter QPC impinge directly on the collector. First, electrons diffract as they emerge from a QPC, with a beam spread of typically $\Theta = 0.25 - 0.45$ *radians* [12], and their path is refocused by the perpendicular field. The effect of the trajectory bend of 180° is to refocus a spreading beam a distance d from width $w \simeq \pi d\Theta$ to $w \simeq \pi d\Theta^2$. As mentioned in section 1.4, in our experiments this refocusing allowed 30% of emitted electrons to be collected at a distance of 1.5 μm away.

A second advantage of the transverse focusing geometry is that trajectories which do *not* enter the collector on the first attempt are reflected off to an irrelevant part of the 2DEG due to the small perpendicular field (and then typically drain to a grounded contact). In the absence of a field, however, those trajectories are backscattered from the collector back to the emitter and lead to interference, which can greatly complicate interpretation of the measurement.

We performed focusing measurements on two kinds of devices: devices in which the emitter was a QPC [13], and devices in which the emitter was a small (0.1 μm^2) quantum dot [14]. The focusing signal was detected as a peak in the collector-base voltage at the focusing condition. The height of a focusing peak (collector *voltage*) reflects the amount of *current*, I_c, that is injected ballistically into the collector. Briefly, this occurs because the collector does not sink current, so that a voltage $V_c = I_c/g_c$ develops between collector and base (g_c is the conductance of the collector point contact). With the collector point contacts kept at or below one channel of conductance, the collector voltage could be written in terms of the transmission of the collector point contact, T_c (≤ 1), as $V_c = (2e^2/h)^{-1} I_c/T_c$ in the spinless case.

To analyze how spin polarization affected the base-collector voltage, we assume $I_{\downarrow c} + I_{\uparrow c} = \alpha(I_{\downarrow e}T_{\downarrow c} + I_{\uparrow e}T_{\uparrow c})$, where $I_{\uparrow,\downarrow e}$ are the spin-resolved emitter currents, α is a spin-independent efficiency parameter reflecting imperfections in the focusing process such as scattering from impurities ($0 < \alpha < 1$), and $T_{\uparrow,\downarrow c}$ are the different collector transmissions

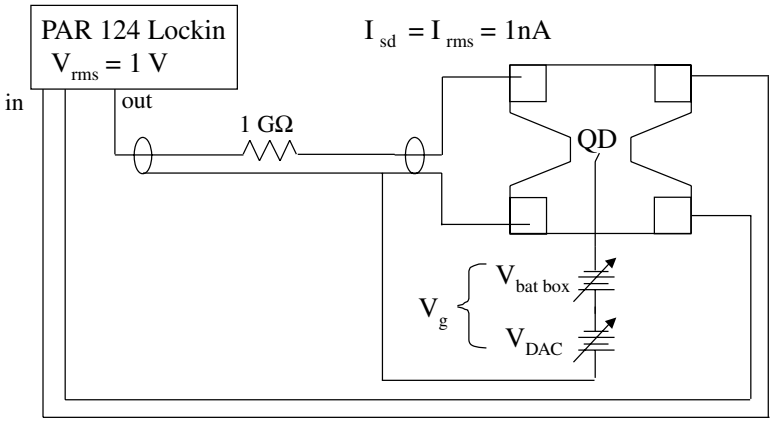

Figure 1.4: Current bias setup, showing the lock-in together with a large ($1G\Omega$ resistor is shown here) resistor used to source a current. If there was a reasonable possibility of the dot accidentally being placed in a high-resistance regime the voltage from the lock-in was in general reduced to 0.1V or even below, and the current bias resistor likewise reduced to maintain the same current.

of the two spin species. In the absence of spin effects ($T_{\uparrow c} = T_{\downarrow c}$), one then expects V_c to be independent of g_c, $V_c = (2e^2/h)^{-1}\alpha I_e$, although different settings of the point contact in practice affects α. Including spin effects, V_c depends only on emitter polarization, $P_e = (I_{\uparrow e} - I_{\downarrow e})/(I_{\uparrow e} + I_{\downarrow e})$, and collector sensitivity $P_c = (T_{\uparrow c} - T_{\downarrow c})/(T_{\uparrow c} + T_{\downarrow c})$ [13, 16],

$$V_c = \alpha \frac{h}{2e^2} I_e (1 + P_e P_c). \tag{1.3}$$

When I_e is held fixed by an emitter current bias, V_c is independent of the emitter conductance, g_e. If instead an emitter voltage bias is applied, only the ratio V_c/I_e will be independent of emitter conductance.

1.7 Measurement Schemes

For the experiments described in sections 2.2, 4.2, and 4.4, standard 2-wire voltage-bias and 4-wire current-bias setups were used. These are described in Figs. 1.3 and 1.4. The experiments described in sections 3.2 and 3.3 used a more complicated 3 lock-in, 6-wire, measurement scheme in which the conductances of emitter and collector as well as the focusing signal could be simultaneously measured; this is shown in Fig. 1.5(a). Here, a current bias ($1\ nA$ or $0.5\ nA$) was applied at $17\ Hz$ across the emitter, while a current bias ($1\ nA$ or $0.5\ nA$) at $43\ Hz$ was applied across the collector, with the base region

grounded. The emitter conductance (proportional to inverse base-emitter voltage V_{BE}^{-1} at 17 Hz), collector conductance (proportional to inverse base-collector voltage $V_{BC}^{-}1$ at 43 Hz), and the focusing signal (V_{BC} at 17 Hz) could then all be determined simultaneously by independent lock-in measurements. The amplitude of the current bias across the collector did not affect the focusing signal.

The measurements reported in section 4.5 required the use of a voltage bias, and therefore a slightly different measurement configuration. This is shown in Fig. 1.5(b). Here, the bias was again applied across the emitter but now the current draining into the base region was measured directly. For this configuration the collector conductance was not measured simultaneously, but rather monitored before and after the focusing measurements using a current bias, to ensure that the conductance had not drifted. The bias (current or voltage) was in all cases chosen to be small enough to ensure that measurements reflected the low-bias, low-temperature limit of conductance for both the emitter and collector.

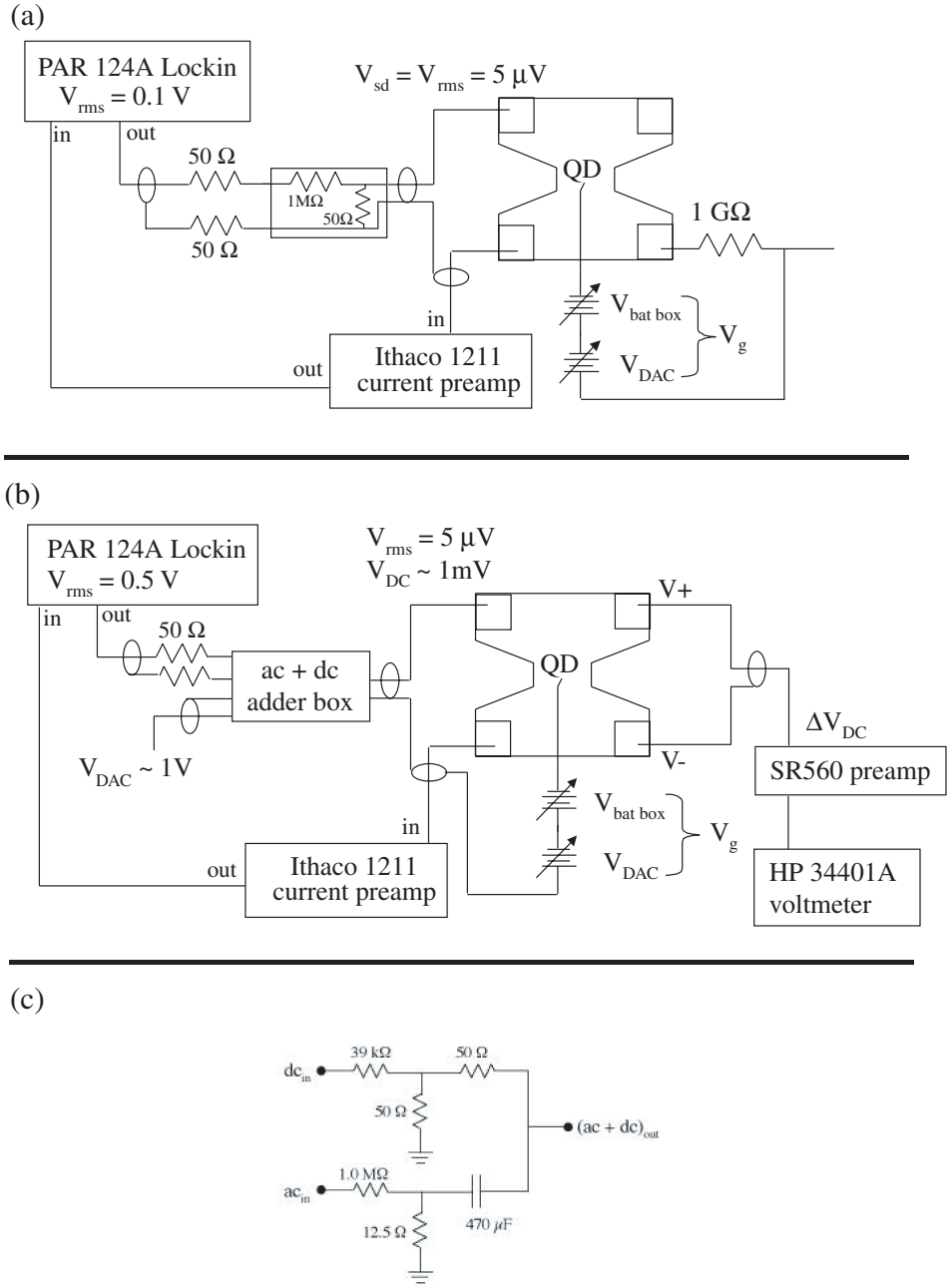

Figure 1.5: (a) Standard voltage bias setup, showing lock-in with voltage divider used to source voltage and Ithaco current preamp used to measure current. The necessity of the $1G\Omega$ resistor used to define ground for the gates was not clear for all measurements, although care had to be taken to prevent current leakage out of that contact. The purpose of the 50Ω resistors on both the ground and inner wire of the lock-in source voltage was to remove a slight voltage on the lock-in ground (about 20 μV) at the lock-in frequency, relative to a real (independent) ground. (b) Same as above, with the addition of an a.c + d.c. voltage adder (c) that allowed the a.c. lock-in signal to be combined with a d.c. voltage from computer digital-to-analog converters. Voltage division of 10^{-5} and 10^{-3} was performed for a.c. and d.c. respectively inside the adder. The adder box was tuned to work at a certain frequency (13 Hz), although its performance was not sharply sensitive to frequency. Circuit diagrams for the battery boxes and DAC circuitry may be found in [3].

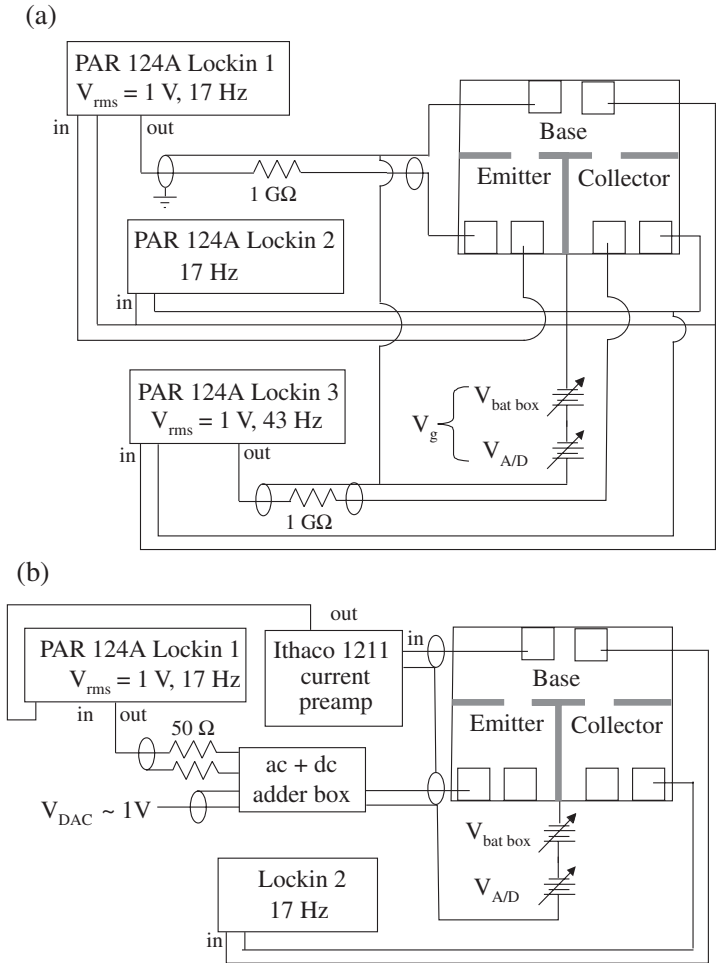

Figure 1.6: (a) Three lock-ins, at two frequencies, were used to measure emitter conductance, collector conductance, and focusing signal simultaneously in a emitter current bias configuration. Currents were biased across the emitter and collector independently, with the base region grounded. (b) Two lock-ins were used to measure emitter conductance and focusing signal simultaneously in a emitter voltage bias configuration. The bias voltage was applied across the emitter with the base region grounded, and collector voltage and emitter current were measured. For (a) and (b), the exact location of the current and voltage ohmics in each region is not accurately depicted, although it affected the hall signal that was present on top of the focusing signal in a trivial but detectable way.

Chapter 2

Spin Degeneracy and Spin Orbit in Open Quantum Dots

2.1 Introduction

Until recently, fully open systems in non-magnetic $GaAs$ heterostructures were assumed to maintain a nearly complete spin degeneracy. For example, at zero magnetic field conductance plateaus in quantum point contacts occur at integer multiples of $2e^2/h$, with the factor of 2 coming from spin degeneracy [15] (although as they are pinched off even point contacts have been shown to exhibit many of the features of a broken spin degeneracy [17, 18]). In this experiment, we set out to help answer the question of where in mesoscopic systems clear spin degeneracy exists fully, with a subsequent even/odd filling of energy levels, and where an exchange interaction exists that favors higher spin states. Already at the time of this experiment, the question of spin filling schemes in confined systems had been the subject of much recent work, but no clear consensus had emerged. Some experiments found evidence of even/odd filling [19, 20], while others found evidence of an exchange interaction [17, 21, 22, 23, 24]. An exchange interaction due to electron-electron interactions would be consistent with recent theoretical work [2, 25, 54].

Those experiments, carried out in transport measurements of Coulomb-blockaded dots, generally probed the spin states of a few discrete energy levels [19, 21, 22, 24, 26]. However, this approach typically provides information about only a small sample of the level spectrum and its spin structure, making results difficult to interpret in general terms. For disordered or chaotic systems, it is often useful to take a statistical approach to spectral and transport

properties [27, 28, 29].

We adopted this strategy, using the statistics of conductance fluctuations to investigate the degree of spin degeneracy in open quantum dots. Open quantum dots are a system lying between fully open mesoscopic systems such as quantum point contacts and fully confined systems such as nearly-isolated quantum dots in the Coulomb blockade regime. The goal here was to use conductance fluctuations in these dots as a probe of spin degeneracy, by looking at how the variance of the fluctuations was affected by the Zeeman splitting induced by an external in-plane magnetic field.

However, the experiment presented in this chapter is an example of one of those cases where the consequences and scientific value of a measurement far exceed the hopes or expectations of even the experimentalists themselves. The data obtained in the course of these measurements, taken together with new theory developed to help explain that data, showed that a spin-orbit interaction, which had previously been considered to be negligibly weak in these systems, was in fact playing a substantial role at large in-plane fields. As a result, considerable theoretical and experimental work has since been undertaken to help to understand the role of spin-orbit interaction in $GaAs/AlGaAs$ dots, and hopefully in the future this will lead to an ability to perform spin manipulations that might otherwise be difficult or impossible.

2.2 Spin in Open Dots: Experimental Results

If a quantum dot system were spin degenerate at low field, then a large in-plane field which lifted the degeneracy via Zeeman splitting would result in changes in the amplitude of conductance fluctuations. If, on the other hand, spin degeneracy at low field were already lifted by interactions, then adding a large Zeeman energy with a parallel field would not alter spectral statistics and hence conductance fluctuation amplitude. It was this decrease in fluctuation amplitude that we were looking for as a signature of zero-field spin degeneracy (see Fig. 2.1).

Surprisingly, we found that the conductance fluctuations were indeed suppressed by a strong parallel field (suggesting degeneracy at low field), but in many cases by a significantly greater factor than could be understood in terms of a simple breaking of spin degeneracy. This greater-than-expected factor of suppression of conductance fluctuation amplitude has now been explained theoretically as the result of a field-dependent spin-orbit scattering,

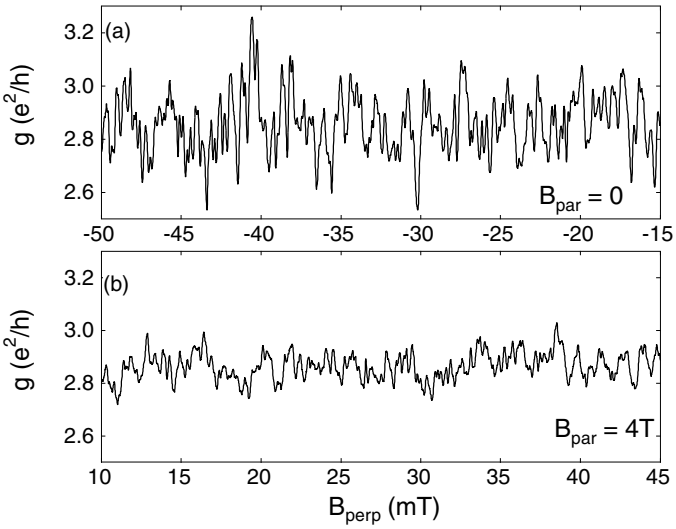

Figure 2.1: A sample of conductance fluctuations in one of the $8\,\mu m^2$ dots, as a function of perpendicular field, B_{perp}, at (a) zero parallel field, $B_{par} = 0$, and (b) $B_{par} = 4T$. Horizontal axes represent field applied through perpendicular coils only; different ranges compensate for small perpendicular component of $4T$ field in (b), and thus represent the same actual perpendicular field.

and has led to further work [33, 31].

The scattering matrix that describes linear transport through an open quantum dot in the presence of spin degeneracy has the form $\left(\begin{smallmatrix} a & 0 \\ 0 & a \end{smallmatrix}\right)$. When that degeneracy is broken, the matrix takes the form $\left(\begin{smallmatrix} a & 0 \\ 0 & b \end{smallmatrix}\right)$, where a and b are scattering matrices for the separate spin channels. Assuming independent random-matrix statistics for a and b (appropriate for disordered or chaotic systems), the variance of conductance fluctuations in dots is calculated to be two times larger for spin-degenerate scattering matrices than for scattering matrices with broken spin degeneracy, irrespective of the number of open channels [31, 34].

A description of mesoscopic conductance fluctuations in terms of the statistics of broadened energy levels of the dot provides an intuitive picture of how conductance fluctuation variance may depend on spin degeneracy [35]. At low temperature, transport occurs coherently through a number of levels proportional to the escape rate from the dot, $\Gamma_{esc}/\hbar$. If levels corresponding to different spins did not mix, only levels of a single spin species would show level repulsion with respect to each other. In this situation, each of the

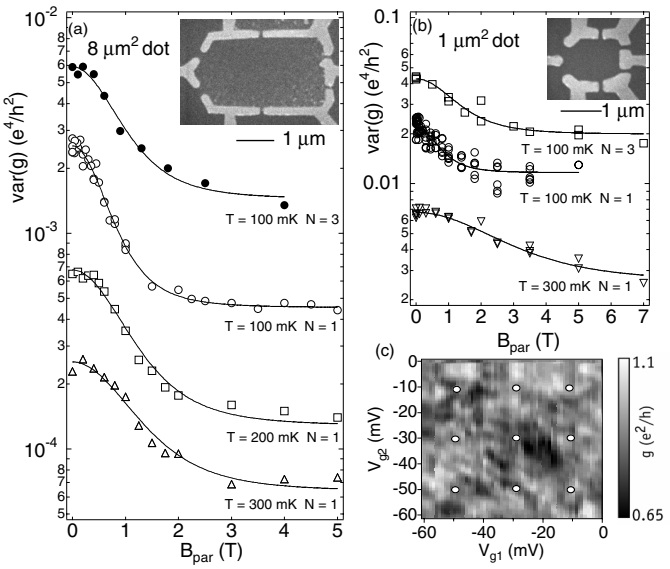

	8 μm²				1 μm²			
	N=1 100mK	N=3 100mK	N=1 200mK	N=1 300mK	N=1 100mK	N=3 100mK	N=1 300mK	N=3 300mK
Reduction Factor	5.5	4.2	5.3	4.0	1.9	2.2	2.6	2.7
Char. Field	0.9T	1.2T	1.4T	1.6T	1.1T	1.9T	3.9T	4.7T

Figure 2.2: Variance of conductance fluctuations, $var(g)$, as a function of parallel field, B_{par}, for (a) an $8\,\mu m^2$ dot and (b) a $1\,\mu m^2$ dot, at several temperatures, T, and numbers of modes, N, in each lead. Fits to a Lorentzian-squared form (solid curves) were used to extract the magnitude and characteristic field for the reduction in $var(g)$. Changes in the magnitude of $var(g)$ as a function of temperature reflect thermal averaging and dephasing. (c) Conductance (greyscale) versus shape-distorting gate voltages V_{g1} and V_{g2} in an $8\,\mu m^2$ device, showing sampling in shape space (white dots) relative to characteristic scale of fluctuations. (Several hundred samples are used to find each value of $var(g)$; see text.) Table: Reduction factors of $var(g)$, and characteristic parallel fields, from Lorentzian-squared fits.

two spin species would contribute $\sim e^2/h$ to conductance fluctuations. When the spectrum is spin degenerate, fluctuations from the two spin species add constructively, giving $var(g) \sim (2e^2/h)^2$. When spin degeneracy is broken, fluctuations instead add randomly, giving $var(g) \sim 2(e^2/h)^2$. It was this factor-of-two difference, between $(2e^2/h)^2$ and $2(e^2/h)^2$ that we were looking for as a signature of spin degeneracy. If the spins do mix, on the other hand (if there is a term in the hamiltonian that mixes spin up and spin down states), then all the levels together contribute $\sim e^2/h$ to conductance fluctuations, leading to a reduction by a factor of roughly 4 from the spin-degenerate, no mixing, case. Finite temperature reduces $var(g)$ by a factor kT/Γ_{esc}, regardless of degeneracy [31].

A reduction of $var(g)$ due to magnetic-field-induced Zeeman splitting was observed previously in disordered mesoscopic systems. In contrast to the observations described in this thesis, both metal [36] and $GaAs$ heterostructure [37] samples showed only the factor of two reduction expected for spin-degenerate transport.

The dots in this experiment were connected to electron reservoirs via leads (point contacts) that passed one or more fully transmitting channels. As described in section 1.6.1, conductance through such a dot at low temperaure fluctuates randomly as a function of various external parameters such as perpendicular magnetic field or device shape. Because conductance fluctuations reflect spectral statistics, they are sensitive to both time reversal symmetry—this aspect was investigated in detail in previous work, Refs. [38, 39, 40]—as well as spin degeneracy in the system. To avoid the complicating effects of a parallel field on time-reversal symmetry, measurements were carried out *in all cases* with a small perpendicular field applied (after confirming that the effect of a perpendicular field in these devices was consistent with previous results [38, 39, 40]).

Devices were fabricated on the material (CEM2385A) described in section 1.4. Measurements were made on three devices, one with area 1 μm^2 (Dot B) and two with area 8 μm^2 (Dot A) (Fig. 2.1(a) and (b), insets), containing roughly 2×10^3 and 1.6×10^4 electrons respectively. Standard 4-wire lock-in techniques were used to measure conductance, with voltage across the sample always less than kT/e. In all cases, noise was less than one tenth of conductance fluctuation amplitude. We used the magnet construction described in section 1.3 to generate the fields necessary for this experiment. The function of the split-coil perpendicular field magnet was, as mentioned before, to break time-reversal symmetry in all cases and to provide additional ensemble statistics for measuring conductance fluctuation variance. In order to minimize the effects of slight changes in temperature, the dilution refrigerator used in these measurements was actively temperature-controlled at 100 mK.

Statistics of conductance fluctuations were gathered over ensembles of dot shapes, created by changing the voltages applied to two shape-distorting gates while the point contacts were simultaneously adjusted to maintain constant transmission. For measurements of $var(g)$ at high temperature and high parallel field, where the fluctuation amplitude was small, the tuning of point contact transmission became especially important because even a small background shift in the point contact transmission could give a misleadingly high value for the variance when taken of an ensemble of shapes. For this reason the tuning of point contact transmission was generally done at very high temperature ($\sim 400mK$).

At each parallel field, variance was measured at several different perpendicular fields, all shown together in Fig. 2.2. An example of conductance fluctuations as a function of two gate voltages is shown in Fig. 2.2c. In the 1 μm^2 dot, 450 shapes were sampled at each field, of which $\sim$ 200 were considered statistically independent; in the 8 μm^2 dot, 900 shapes were sampled, of which $\sim$ 450 were considered independent. Again, all ensembles were taken with a perpendicular field sufficient to break time-reversal symmetry in the devices.

The amplitude of conductance fluctuations was found to decrease and then saturate upon application of a parallel field of several tesla in all cases, as seen in Fig. 2.2. In most cases the reduction was significantly larger than the expected factor of two from spin degeneracy (see Table in Fig. 2). In both 8 μm^2 devices, $var(g)$ decreased by a factor of $\sim$ 4 to 5; in the 1 μm^2 dots, $var(g)$ decreased by a factor of $\sim$ 2 at the lowest temperatures and $\sim$ 3 at higher temperatures. The field scale for the reduction of $var(g)$ increased with the number of channels in the point contacts and with temperature (see Fig 2, table). Over the same range of parallel field, *average* conductances typically changed by less than 5%.

We were able to rule out the possibility that the reduction in $var(g)$ at high parallel field was caused by increased temperature or increased dephasing, either of which would suppress conductance fluctuations, by measuring those two directly [39, 41]. First, a direct measurement of electron gas temperature using Coulomb blockade peak width indicated that for $T \geq 100mK$ a parallel field of $4T$ increased electron temperature by $< 5\%$, relative to zero field.

To compare dephasing rates at low and high fields, we could not use the standard measure of dephasing—the magnitude of the weak localization correction to average conductance —because fields larger than $\sim 0.5T$ were observed to break time-reversal symmetry even when strictly parallel to the plane of the heterostructure. (This is an effect studied further in Ref. [33].) Instead, dephasing rates were compared using power spectra of magnetoconductance fluctuations, which for chaotic dots have the form $S(f) \propto e^{-f/f_0}$, where f is the frequency in cycles/mT, $f_0 \propto (N + \pi\hbar/(\Delta\tau_\varphi))^{-1/2}$, Δ is the level spacing of the dot, and τ_φ is the dephasing time [42, 43]. Note that the characteristic frequency f_0 has no explicit temperature dependence but does depend on τ_φ. This measure of dephasing rate has been shown to be consistent with weak localization measurements in quantum dots above $300mK$ [40].

Power spectra of conductance fluctuations at low and high parallel field, as well as at higher temperature, are shown in Fig. 2.3. All spectra clearly show the expected e^{-f/f_0}

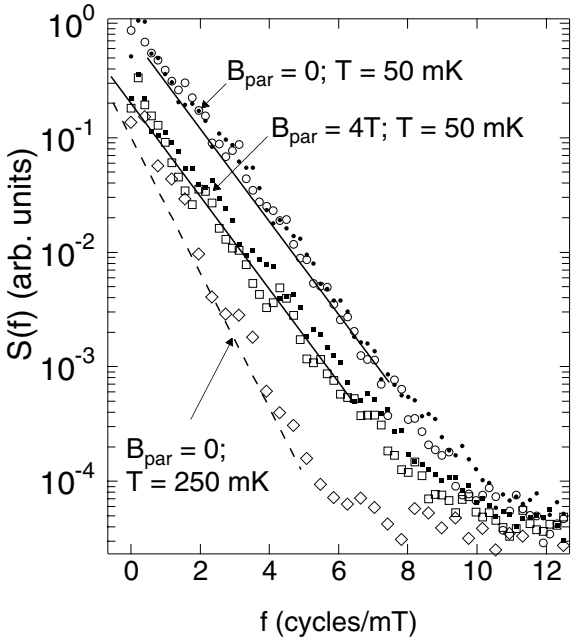

Figure 2.3: Power spectra $S(f)$ of conductance fluctuations in an 8 μm^2 dot at $B_{par} = 0$ for $50mK$ (circles) and $250mK$ (diamonds), and at $B_{par} = 4T$ for $50mK$ (squares). Open and filled markers show different shape ensembles. $S(f)$ has the expected exponential form (see text), with characteristic frequency f_0 given by the slope in the log-linear plot. Identical slopes at $B_{par} = 0$ and $4T$ (parallel solid lines) indicate no change in dephasing at high field. The steeper slope of $S(f)$ at $250mK$ (dashed line) indicates increased dephasing.

form, with the steeper slope for the $250mK$ data showing that f_0 is indeed sensitive to dephasing. From the high-field curve we observe that f_0 at $B_{par} = 4T$ is certainly not smaller than—and perhaps is even slightly larger than—the value at zero parallel field, suggesting that the dephasing rate has not increased at large parallel field.

With time-reversal symmetry already broken by a perpendicular field, orbital effects due to a parallel field—including wave function compression or flux coupling due to a rough or asymmetric quantum well—should not affect $var(g)$. Having eliminated field-dependent temperature, decoherence, and orbital coupling as causes of the reduced $var(g)$, one is led to suspect that the effect may be spin related. Recalling the original motivation for the measurement, the reduction in $var(g)$ implies spin degeneracy at low field, up to an energy resolution $\epsilon \sim max(\Gamma_{esc}, kT)$, within the simple picture discussed above. However, the fact that $var(g)$ is reduced by considerably more than the expected factor of two with no increase in dephasing means that this simple picture must be incomplete. Another difficulty with the

model of broken spin degeneracy is that the expected field scale for reducing $var(g)$ should be given by $g\mu B \sim \epsilon$. However, for the 8 μm^2 dot, where $\Gamma_{esc} \ll kT$ for all temperatures measured, the field scale for the reduction was found not to be proportional to temperature (see Table 1).

A reasonable interpretation of the suppression of $var(g)$ at high fields beyond a factor of two is that there is a greater degree of spectral rigidity at high field than can be accounted for by Zeeman splitting of spin-degenerate levels. As has been pointed out by several authors, a mechanism that could lead to this enhanced rigidity is spin-orbit scattering, which would cause *all* levels in the spectrum to repel, and thereby lead to the observed factor-of-four decrease in variance. However, the role of spin-orbit scattering in explaining our results is clearly rather subtle. First, the average conductance always shows weak localization rather than anti-localization around zero field over a broad range of temperatures and device areas, indicating that $\tau_{so} > \tau_{\varphi}$ at low fields. Second, if strong spin-orbit scattering were present even at zero parallel field, the perpendicular field necessary to break time-reversal symmetry (present in all of these measurements) would have been sufficient to suppress $var(g)$ fully, and no further change would have been observed as a function of parallel field. If, however, spin-orbit scattering increased upon application of a parallel field (leaving spin-degeneracy intact at low field) one would expect a suppression in $var(g)$ at high parallel field of greater than a factor of two while still observing weak localization (rather than anti-localization) around zero field.

It was this field-dependent spin-orbit interaction that led to further work. Interestingly, the factor-of-*two* reduction of $var(g)$ found in the 1 μm^2 dot was now also difficult to explain, and but probably involved a dependence of these effects on device size. In the few years since this work took place, these effects have been explained thoroughly in new theoretical and experimental work. [30, 31, 32, 33].

Chapter 3

Polarization Fluctuations in an Open Dot

3.1 Introduction

The results presented in the previous chapter lead to a rather interesting, if straightforward, conclusion: the two independent spin channel conductance fluctuations that, taken together, give rise to a factor-of-two suppression in overall conductance fluctuation variance when spin degeneracy is broken would also give rise to fluctuations in the polarization of transport electrons. The reason that the two spin channels undergo different conductance fluctuations is, essentially, that the two are separated by a Zeeman energy, therefore have different Fermi wavelengths, and therefore see different interference patterns in transport. Because the transmissions of the two spin channels have mesoscopic fluctuations, there would be places in parameter space where the transmission for spin-up electrons (for example) would be much greater than for spin-down electrons, leading to a strong spin-up polarization in the transport current; the opposite would also be found in other places. It is these mesoscopic fluctuations of polarization in transport electrons that we explore in this chapter.

This is one of the clearest examples in mesoscopic physics of an effect that depends on both phase coherence (leading to the conductance fluctuations) and spin, and it opens the door to many "spintronics" applications that would otherwise not have been possible. Most proposals for spintronics applications rely on the ability to prepare and detect electrons of various spin orientations [44]. Previously, the only way to create spins of either polarity (up or down) was to have switchable ferromagnetic components in the circuit or to allow

for some type of local ESR. Ferromagnetic materials create several problems: first, there are no known ferromagnetic materials with the long mean free path, long phase coherence time and spin-relaxation time, as well as the lithographic flexibility of clean $GaAs/AlGaAs$ systems. Second, reversing the direction of spin polarization in-situ implies reversing the direction of the magnetic field seen by the ferromagnetic material, which takes time and implies associated problems with, for example, stray fields. The effect demonstrated in these experiments, on the other hand, results in spin polarization that can be flipped simply by tuning the voltage on an electrostatic gate.

Completing these measurements was a two stage process. First, we had to develop a technique to detect spin polarization of transport electrons in a clean, non-magnetic 2DEG system. Our demonstration of such a technique is presented in section 3.2. Then, we used this technique to explore the mesoscopically fluctuating spin polarization of current emitted from a small quantum dot; this work is presented in section 3.3.

3.2 Detection of Electron Spin: Experimental Results

The detection of electron spin in mesoscopic systems was the aim of extensive experimental efforts for many years. Unfortunately, the long coherence times [45] that make electron spin interesting arise fundamentally from the weak coupling of spin to the environment, and this makes the task of measuring spin difficult.

In this measurement we demonstrated a technique to measure spin currents by converting the problem into the easier one of measuring currents of electrical charge. As described before, at low field and low temperature a quantum point contact (QPC) [see Fig. 3.1(a)] transmits through two spin degenerate channels, producing conductance plateaus at integer multiples of $2e^2/h$. When a large in-plane magnetic field is applied, the degeneracy is lifted and conductance becomes quantized in multiples of $1e^2/h$ [Fig. 3.1(b)] [46, 47]. While the electrons emitted from an e^2/h plateau are widely believed to be spin polarized, this had not been verified experimentally prior to this work. One key result of these experiments was the demonstration that point contacts do operate as emitters and detectors of spin current, and therefore allow the detection of spin polarization to be accomplished by simply measuring electrical resistance.

Our experiment was based on a technique known as transverse electron focusing [6], described in section 1.6.3. The device geometry shown in Fig. 3.1(a) allowed electrons from

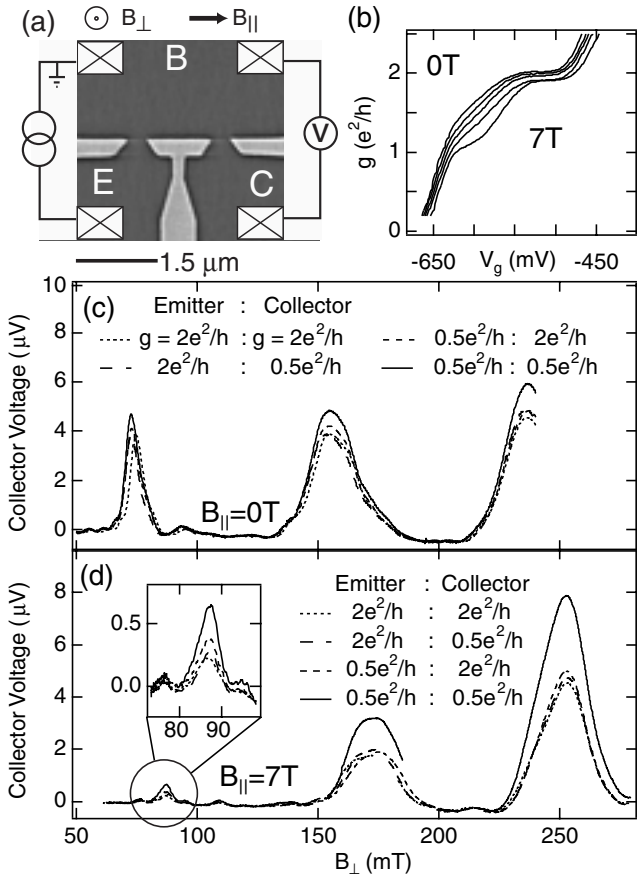

Figure 3.1: (a) SEM micrograph of a device similar to the one measured in this experiment, two quantum point contacts in a transverse focusing geometry with perpendicular ($B_\perp$) and in-plane ($B_\parallel$) magnetic fields oriented as shown. With a fixed current applied between emitter (E) and base (B), the voltage between base and collector (C) showed focusing peaks as a function of $B_\perp$. (b) At $T = 300\ mK$, both point contacts showed conductance quantized in units of $2e^2/h$ at $B_\parallel = 0$, and in units of e^2/h at large $B_\parallel$. (c) At $B_\parallel = 0$, the collector voltage was nearly independent of the conductances of the two point contacts. The last focusing peak is cut off due to current limitations of the perpendicular field solenoid. (d) At $B_\parallel = 7\ T$ the focusing peaks were enhanced only when both emitter and collector are set to $g = 0.5e^2/h$. The enhancement demonstrates that both emitter and detector are spin selective, by Eq. (1.2).

a spin-polarizing emitter—in this case a QPC—to be coupled into a second QPC serving as a spin-sensitive collector. A magnetic field, $B_\perp$, applied perpendicular to the 2DEG plane, bent and focused ballistic electron trajectories from the emitter to the collector, resulting in peaks in the base-collector voltage [Figs. 3.1(c) and 3.1(d)] at the focusing condition, $d = 2Nm^*v_F/eB_\perp$, where m^* is the effective electron mass, v_F the Fermi velocity, and N is any integer.

The coupling efficiency between emitter and collector was quite high in the extremely high mobility 2DEG materials used in this experiment, allowing the two QPCs to be separated by several microns. This separation was one of the primary advances made in this technique, as it allowed spin measurements of the emitted current to be decoupled from the details (often rather complicated, and mesoscopically sensitive to various parameters) of the emitting device under test. This greatly simplified the interpretation of results. A further advantage of a focusing geometry was that spin detection occurred very quickly ($< 10\ ps$) after the polarized electrons were emitted, leaving little time for spin relaxation.

The focusing signal was measured as a voltage between collector and base regions, as described in section 1.6.3. Polarization could be determined from focusing peak height using Eq. (1.2); these measurements were performed using a current bias, so I_e was fixed and changes in the focusing peak height reflected only changes in emitter or collector polarization or changes in focusing efficiency α. Note that, from Eq. (1.2), colinear and complete spin polarization ($P_e = 1$) and spin selectivity ($P_c = 1$) gives a collector voltage twice as large as when *either* emitter or collector are not spin polarized.

The focusing device was fabricated on a high-mobility two-dimensional electron gas (2DEG) formed at the interface of a GaAs/$Al_{0.36}Ga_{0.64}As$ heterostructure, defined using Cr/Au surface depletion gates patterned by electron-beam lithography, and contacted with nonmagnetic (PtAuGe) ohmic contacts. The 2DEG was 26 nm from the Si delta-doped layer ($n_{Si} = 2.5 \times 10^{12}\ cm^{-2}$) and 102 nm below the wafer surface. Mobility of the unpatterned 2DEG was $5.5 \times 10^6\ cm^2/Vs$ in the dark, limited mostly by remote impurity scattering in the relatively shallow structure, with an estimated background impurity level $< 5 \times 10^{13}\ cm^{-3}$. With an electron density of $\sim 1.3 \times 10^{11}\ cm^{-2}$, the transport mean free path was $\sim 45\ \mu m$, much greater than the distance (1.5 μm) between emitter and collector point contacts. The Fermi velocity associated with this density is $v_F = 2 \times 10^7\ cm/s$, consistent with the observed $\sim 80\ mT$ spacing between focusing peaks.

For this experiment, measurements were performed in a ^3He cryostat with a base temperature of 300 mK, rather than in a dilution refrigerator. Using a similar set of magnets to that described in section 1.3, $B_{\|}$ was oriented along the axis between the two point contacts, as shown in Fig. 3.1(a), while the perpendicular field could be tuned to select between focusing peaks.

Independent ac current biases of 1 nA were applied between base and emitter (17 Hz), and base and collector (43 Hz), allowing simultaneous measurement of the emitter conductance, collector conductance, and the focusing signal as described in section 1.7. This measurement setup is described in more detail in Fig. 1.5.

The qualitative behavior of the focusing peaks did not change upon thermal cycling. Although all of the data presented here come from a single device, results were confirmed in a similar device on the same heterostructure. Statistics leading to estimates of typical polarization values discussed at the end of the paper were gathered over five settings of point contact voltages (for fixed conductance) for each of the three focusing peaks. Data from the three focusing peaks showed consistent behavior.

Spin polarized emission and detection were measured by comparing the height of the focusing peak for various conductances of the emitter and collector point contacts. At $B_{\|} = 0$, where no static spin polarization is expected, the focusing signal was found to be nearly independent of the conductances of both emitter and collector point contacts, as shown in Fig. 3.1(c). In contrast, at $B_{\|} = 7\ T$, the focusing signal observed when both the emitter and collector point contacts were set well below $2e^2/h$ was larger by a factor of ~ 1.7 compared to the signal when either emitter or collector was set to $2e^2/h$, as seen in Fig. 3.1(d).

To normalize for overall variations in transmission through the bulk from the emitter to the collector, the focusing signal can be expressed as a ratio normalized by the value when both the emitter and collector are set to $2e^2/h$. We denote the point contact settings as $(x : y)$ where $x\,(y)$ is the emitter (collector) conductance, in units of e^2/h. Ratios are then denoted $(x : y)/(2 : 2)$.

Figures 3.2 and 3.3 show the focusing signal ratios for the third focusing peak ($B_{\perp} \sim 230 - 250\ mT$), chosen because its height and structure in the $(2 : 2)$ condition were less sensitive to $B_{\|}$ and small variations in point contact tuning compared to the first and second peaks. Although all curves shown in this paper were for the third focusing peak, spin polarization extracted from the first and second focusing peaks gave similar results.

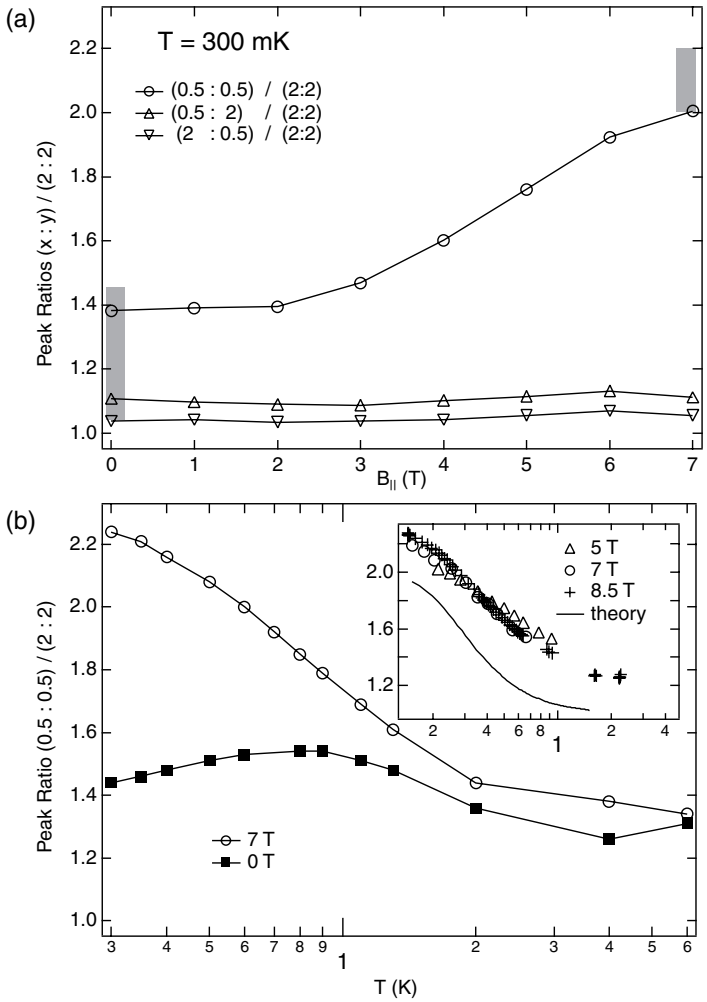

Figure 3.2: (a) The height of the third focusing peak as a function of $B_{\|}$ for different conductances of the point contacts $(x : y)$, where x is the emitter conductance and y is the collector conductance (in units of e^2/h), all normalized by the $(2 : 2)$ focusing peak height. According to Eq. (1.2), a factor of two in the ratio indicates fully spin polarized emission and detection. Grey shaded boxes indicate typical ranges (see text) of $(0.5 : 0.5)/(2 : 2)$ ratio. (b) Temperature dependence of the ratio of focusing signals $(0.5 : 0.5)/(2 : 2)$ for $B_{\|} = 7\ T$ and $0\ T$. (a) and (b) are from different cooldowns. Inset: Ratio $(0.5 : 0.5)/(2 : 2)$ for $B_{\|} = 5, 7$, and $8.5\ T$ plotted as a function of the scaled temperature $kT/g\mu B_{\|}$. The solid curve is the prediction of a simple model (see text) that accounts for only thermal broadening in the leads.

Figure 2(a) shows that only the ratio $(0.5:0.5)/(2:2)$ grows with $B_{\|}$, reaching a value ~ 2 at $7T$, while the other ratios, $(2:0.5)/(2:2)$ and $(0.5:2)/(2:2)$, are essentially independent of in-plane field, as expected from Eq. (1.2) if no spin selectivity exists when the conductance is $2e^2/h$. At $B_{\|}=0$, we find $(0.5:0.5)/(2:2) \sim 1.4$, rather than the expected 1.0, for this particular setting of the point contacts.

Temperature dependences of the $(0.5:0.5)/(2:2)$ ratio are shown in Fig. 3.2(b) for a different cooldown. At $B_{\|}=7T$, the ratio $(0.5:0.5)/(2:2)$ decreases from ~ 2.2 at $T=300\ mK$ to a zero-field value of 1.4 above $2K$. Note that $2K$ is roughly the temperature at which $g\mu B_{\|}/kT \sim 1$, using the $GaAs$ g-factor $g=-0.44$. At $B_{\|}=0$, the ratio $(0.5:0.5)/(2:2)$ remains near 1.4, with only a weak temperature dependence up to $6K$.

The inset of Fig. 3.2(b) shows that the focusing data at several $B_{\|}$ scale to a single curve when plotted as a function of $kT/g\mu B_{\|}$, suggesting that both spin-polarized emission and spin-selective detection arise from an energy splitting that is linear in $B_{\|}$. A simple model that accounts roughly for the observed scaling of the focusing signal assumes that the point contact transmission, $T(E)$, is 0 for $E<E_0$, and 1 for $E>E_0$, where E is the electron kinetic energy and E_0 is a gate-voltage-dependent threshold. Spin selectivity then results from the Zeeman splitting of the two spin sub-bands, and is reduced by thermal broadening. Except for a vertical offset of ~ 0.4, this simple model agrees reasonably well with the data [Fig. 3.2(b), inset].

Fig. 3.3(a) shows the evolution of spin selectivity in the collector point contact as a function of its conductance. At $B_{\|}=6\ T$, with the emitter point contact set to $0.5e^2/h$, the collector point contact is swept from $2e^2/h$ to 0. The focusing signal increases as the collector point contact conductance is reduced below $2e^2/h$, saturating only well into the tunneling regime, below $\sim 0.5e^2/h$. For this reason we use emitter and collector conductances of $0.5e^2/h$ in all figures for the spin-selective cases (although the qualitative behavior of the data was essentially the same here as on the e^2/h plateau). Similar to the effect seen in Fig. 3.2(b), spin selectivity decreases with increasing temperature, approaching the zero field curve at $1.3\ K$.

Fig. 3(b) shows the same measurement taken at $B_{\|}=0$. The focusing peak rises slightly when both point contacts are set below one spin degenerate channel. Unlike at high field, however, the increase of the focusing signal is very gradual as the point contact is pinched off. In addition, temperature has only a weak effect.

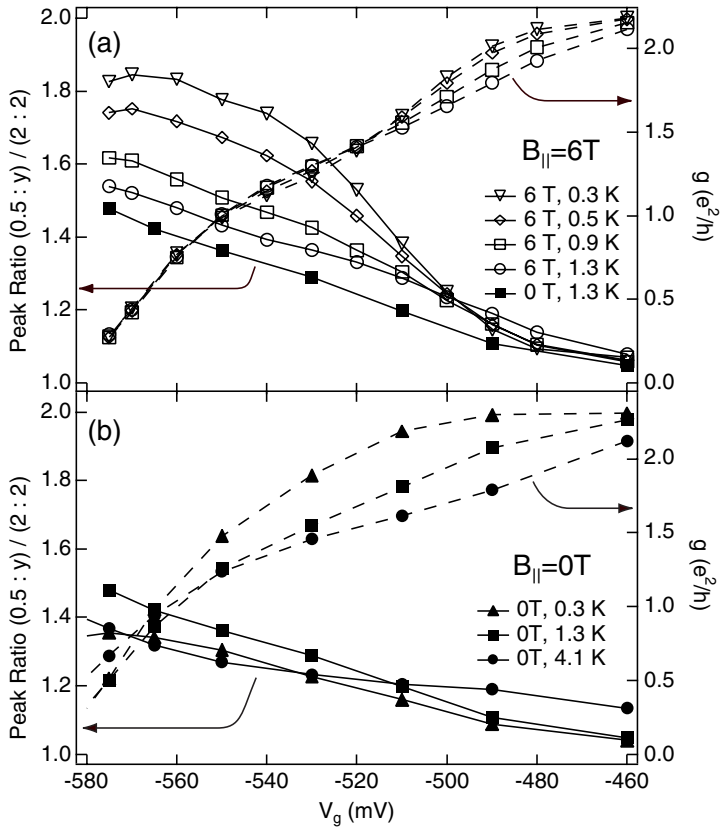

Figure 3.3: (a) Focusing signal ratio $(0.5 : y)/(2 : 2)$ and collector conductance g at $B_{\|} = 6\ T$ as a function of the voltage applied to one of the collector gates, with the emitter fixed at $g = 0.5e^2/h$. This shows the onset of spin selectivity as the collector point contact is brought into the tunneling regime, $g < 2e^2/h$. (b) The same data taken at $B_{\|} = 0$, showing little temperature dependence up to 4 K. A mild 0.7 structure in the conductance becomes more prominent at 1.3 K.

As mentioned above, both the low and high field ratios $(0.5 : 0.5)/(2 : 2)$ were typically measured to be larger than their ideal theoretical values of 1 and 2 respectively. Sampled over multiple thermal cycles, several gate voltage settings (shifting the point contact centers by $\sim 100\ nm$), and different focusing peaks, the ratio at $B_{\|} = 0$ varied between 1.0 and 1.6, with an average value of 1.2 and a standard deviation $\sigma = 0.2$. The average value of the ratio at $B_{\|} = 7\ T$ was 2.1, with $\sigma = 0.1$. This represents an increase from low to high field by a factor of 1.7 ± 0.3, so from Eq. 1 one finds $P_e P_c = 0.7 \pm 0.3$. Because neither P_e nor P_c can be greater than 1, this then implies that both P_e and P_c are greater than 0.7 ± 0.3, and under the assumption that $P_e \sim P_c$ it implies that $P_e, P_c > 0.8$.

Both point contacts display a modest amount of zero-field "0.7 structure" [17, 18], as seen in Figs. 3.1(b) and 3.3(b). Although a static spin polarization associated with 0.7 structure would be consistent with our larger-than-one ratio $(0.5 : 0.5)/(2 : 2)$ at zero field, this explanation is not consistent with an enhanced ratio found *both* at zero field and high field. Rather, we believe the enhancement is due to a slight dependence of α on QPC settings in the regime $(T_c, T_e) < 1$. This explanation is consistent with the weak temperature dependence of the zero-field ratio up to 4 K.

In summary, we demonstrated that a point contact at high field on the $1e^2/h$ plateau does indeed emit spin polarized current, and more importantly we showed that we were able to detect the spin-polarization of that current in a different device. Therefore we are ready to proceed in the next section to measuring spin polarization from structures with a more complicated behavior than point contacts.

3.3 Spin Filtering by Quantum Interference

The transport behavior of an open quantum dot is closely tied to quantum interference of the electrons participating in that transport, and this leads to a considerably greater subtlety in the spin structure of a quantum dot compared with a quantum point contact. A point contact can be set to pass current that is either spin polarized or unpolarized, but cannot have the direction of the polarization reversed. Basically, the reason for this is that quantum point contacts are "high-pass" kinetic energy filters. They can be set to transmit the higher energy spin (lower potential energy, but after thermalization a higher kinetic energy) while blocking the lower energy spin, but can never be set to transmit the lower energy spin but block the higher energy spin. A quantum dot, on the other hand, is at low temperatures essentially an energy "band-pass" filter. The transmission coefficient—due to interference—for electrons depends sensitively on their kinetic energy, but not in a consistent way: at some settings the dot will pass electrons of higher energy but not electrons of lower energy, and at other settings it is the other way around. As mentioned in the introduction this means that at high field quantum dots may be expected to pass *either* one spin or the other based in the exact setting of mesoscopic parameters.

We refer to such flexibility in a spin filter as *tunability*. The development of tunable spin filters in other systems has been the goal of many research programs over the last several years. Some notable successes have already been achieved: spin polarizations of $\sim 15\%$ from

all-metal devices using ferromagnetic spin injectors have been reported [48, 49], and spin injection from ferromagnetic semiconductors into normal semiconductors has been reported with polarizations of up to 90% [50, 51].

The goals of our effort were to realize such highly selective filters in a clean, quantum coherent system, and furthermore to use gate voltages to control the orientation of the filter without needing to reverse externally applied magnetic fields. As with point contacts, the filtering properties of a dot should in principle be able to be changed by adjusting the voltage on electrostatic gates. Fast gating techniques developed in conventional microelectronics could then be used to produce rapidly activated filters without having to change the applied magnetic fields.

In this experiment we demonstrated, by directly measuring the spin polarization of emitted current, a mesoscopic spin filter in our $GaAs/AlGaAs$ heterostructure system that (i) maintained quantum coherence, (ii) achieved significant (up to $\sim 70\%$) polarization, and (iii) could be turned on and off, and reversed in polarity, using small (few mV scale) gate voltages without changing the external magnetic field. The spin filter consisted of a small (~ 100 electron) lateral quantum dot in a $GaAs/AlGaAs$ heterostructure [see Fig. 3.4(a)]. At low temperatures, such dots are known to exhibit universal conductance fluctuations (UCF) [52] resulting from quantum interference of coherent transport paths. In an in-plane magnetic field, the different Fermi wavelengths of spin-up and spin-down electrons led to different interference patterns for opposite spin directions. The dot could therefore be tuned using gate voltages to configurations where the transmission of one or the other spin was strongly suppressed by destructive interference, thus forming a tunable spin filter.

Spin filtering properties were measured in a polarizer/analyzer geometry as in the QPC experiment discussed in the last section, where the spin polarization of current emitted from the dot (the polarizer) in an in-plane field, $B_{\|}$, was detected using a QPC at $0.5e^2/h$ (the analyzer) [see Fig. 3.4(a)] [13]. As before, the polarizer and analyzer elements were coupled by transverse focusing using a small perpendicular magnetic field, $B_{\perp}$ [6, 13]. With constant current flowing between the emitter and base regions, focusing peaks (i.e., peaks in the collector-base voltage, V_c) were again observed at the appropriate fields (integer multiples of 80 mT). Here data is presented for the second focusing peak (at ~ 160 mT, see Fig. 3.4(b)), with others showing consistent behavior.

In an in-plane field, the height of a focusing peak reflects the degree of spin polarization of the emitted current whenever the detector QPC conductance, g_c, is in a spin-selective

regime, $g_c < e^2/h$, as discussed previously. Again, the dependence of the focusing peak height on spin polarization is given by Eq. (1.2).

The device used in this experiment was fabricated on the same 2DEG as the device discussed in the previous section, remarkable for its high mobility. Unlike in the previous section, measurements were performed in a dilution refrigerator with base electron temperature of 70 mK. Again, a standard superconducting solenoid was used to generate the in-plane field, while an independent superconducting coil was used to generate perpendicular magnetic fields.

Figure 3.4(c) and 3.4(d) show focusing peaks measured at $B_{\|} = 6\ T$ with a spin-sensitive ($g_c = 0.5e^2/h$) collector. In Fig. 3.4(c), two of the gates forming the dot were undepleted, making the emitter a single QPC set at $2e^2/h$ [see Fig. 3.4(c) inset] as in the previous section. One does not expect spin polarization in the emitter current from a QPC to fluctuate with plunger gate voltage. As anticipated, the height of the focusing peak remains constant. In contrast, Fig. 3.4(d) shows the situation when all gates were depleted, so that a dot was formed at the emitter with both leads of the dot set to $2e^2/h$. In this case, quantum interference within the dot (also the source of conductance fluctuations) is expected to give rise to fluctuations in the spin polarization of the emitted current, even though the leads of the dot are not polarizing. These mesoscopic fluctuations of spin current polarization appear as fluctuations in the focusing peak height in Fig. 1(d). We emphasize that the total emitted current was held fixed using a current bias, and did not fluctuate as the dot conductance changed. Note that the focusing peak *position* also does not change as a function of plunger voltage, allowing peak height fluctuations to be measured at fixed $B_{\perp}$.

The rest of this section explores in detail the spin-filter effect described above. Figure 3.5 demonstrates that the focusing peak height fluctuations observed were indeed due to fluctuations in spin, by showing that focusing fluctuations disappear when either the collector is insensitive to spin ($g_c = 2e^2/h$) or Zeeman splitting is reduced to zero. Figure 3.5 also demonstrates that the filter is bipolar, controlled by a gate. Having demonstrated that an open dot in an in-plane field acts as a bipolar spin filter when its leads are *not* spin selective (i.e., when set to $2e^2/h$), we show in Fig. 3.6 the effect of making the exit point contact of the dot also act as a spin filter. The result is that the combined dot-filter plus QPC-filter can no longer be set to preferentially pass the higher-energy spin direction. This will have ramifications for the Coulomb blockade measurements presented in Chapter

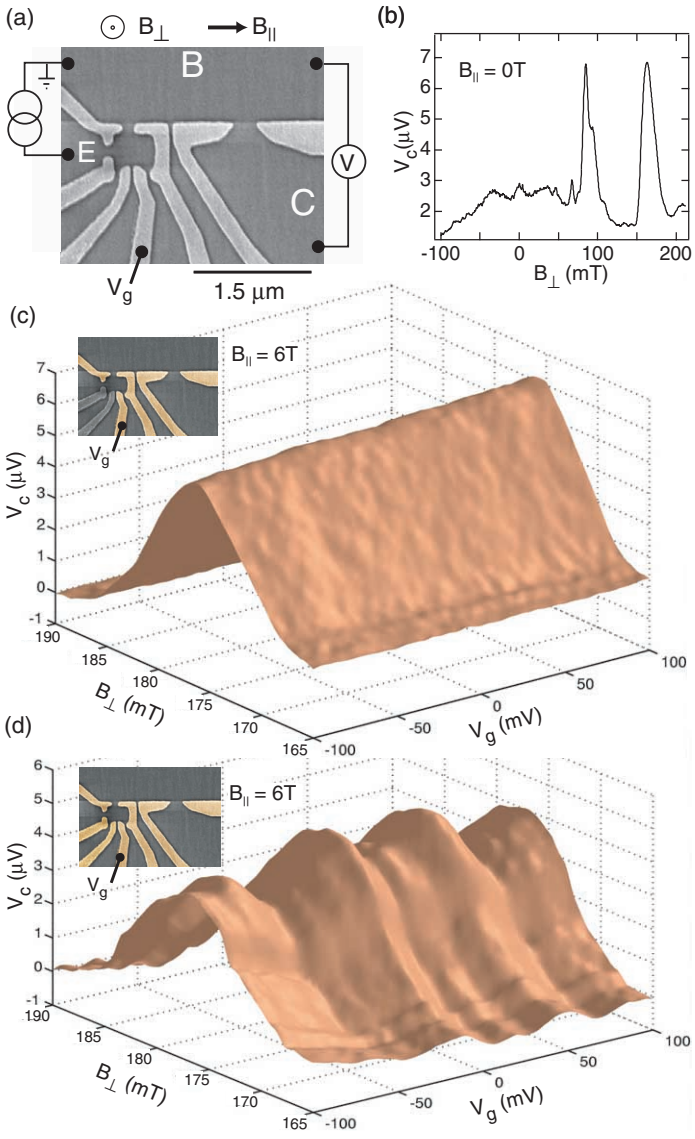

Figure 3.4: (a) Micrograph and circuit showing the polarizer/analyzer configuration used in the experiment. The emitter (E) can be formed into either a quantum dot or a point contact. The collector (C) is a single point contact. Electrons are focused from emitter to collector through the base region (B) using a small perpendicular magnetic field. (b) Base-collector voltage, V_c, showing two focusing peaks. (c,d) Focusing peak as a function of plunger gate voltage, V_g, with spin-selective collector ($g_c = 0.5e^2/h$). Small background Hall voltage is subtracted off. (c) Emitter is single QPC at $2e^2/h$, (d) Emitter is quantum dot, with both leads at $2e^2/h$. Fluctuations in focusing are not sensitive to conductance fluctuations, as the current is held fixed. Rather, focusing peak fluctuations reflect fluctuations in spin polarization of emitted current.

4. In Fig. 3.7, we return to unpolarized QPC's in the dot and compare the statistics of spin polarization of the emitted current to a simple random matrix theory model [53].

Figure 3.5(a) shows focusing peak heights at $B_{\|} = 6\ T$ with a spin-selective collector ($g_c = 0.5e^2/h$) for the cases of either a dot or a QPC as emitter. With the emitter configured as a single QPC on the $2e^2/h$ plateau (black curve) the focusing peak shows only weak fluctuations as a function of a plunger gate voltage. This is the control case of unpolarized emission, $P_e = 0$. When the dot is fully formed (red curve), fluctuations in the focusing peak height extend *both above and below* the unpolarized curve, demonstrating that the polarization P_e shows mesoscopic fluctuations around zero. That is, the polarization may be either aligned or anti-aligned with the applied field, depending on the plunger gate voltage.

Focusing peak heights (normalized by their averages) are shown in Fig. 3.5(b) under various polarization conditions of emitter and collector. The red curve shows bipolar spin current fluctuations when the dot was formed and the collector was spin selective ($g_c = 0.5e^2/h$) at $B_{\|} = 6\ T$. Removing the spin sensitivity of the collector by setting $g_c = 2e^2/h$ caused the fluctuations to disappear (green curve). At $B_{\|} = 0$, fluctuations were also absent, irrespective of g_c (blue curve). In all cases, fluctuations in conductance remained large [see Fig. 2(c)], verifying that the spin-dependent focusing peak fluctuations were not due to UCF.

In order to extract quantitatively the spin polarization of emitted current, P_e, we first measured the collector sensitivity, P_c, also less than one due to finite temperature and mode mixing. To find P_c, we configured the emitter as a single QPC and compared focusing peak heights at $B_{\|} = 6T$ and $g_c = 0.5e^2/h$ for the two cases $g_e = e^2/h$ and $g_e = 2e^2/h$. Fully polarized emission and detection would give peak heights differing by a factor of two (see Eq. (1.2)), whereas we found a factor of 1.5 (see Fig. 3.6a inset). Assuming the point contacts have equal polarization gives a value $P_c = P_e = \sqrt{1.5 - 1} \sim 0.7$. The rather poor quality of the collector QPC relative to the emitter (see Fig. 3.6b, right inset) suggests that P_c is in fact less than P_e. Using the value $P_c = 0.7$ to convert focusing signals to emitter polarizations, P_e, in Fig. 3.5(a) and Fig. 3.7 therefore provides conservative estimates of P_e.

Figure 3.6 shows fluctuations of emitter polarization as the conductance of the exit QPC of the dot in the emitter (see Fig. 3.6(b), left inset) is reduced below $2e^2/h$, with the entrance QPC held fixed at $2e^2/h$. The upward trend in polarization as the exit QPC is closed shows that a dot that can generate polarizations in both directions when both leads are open

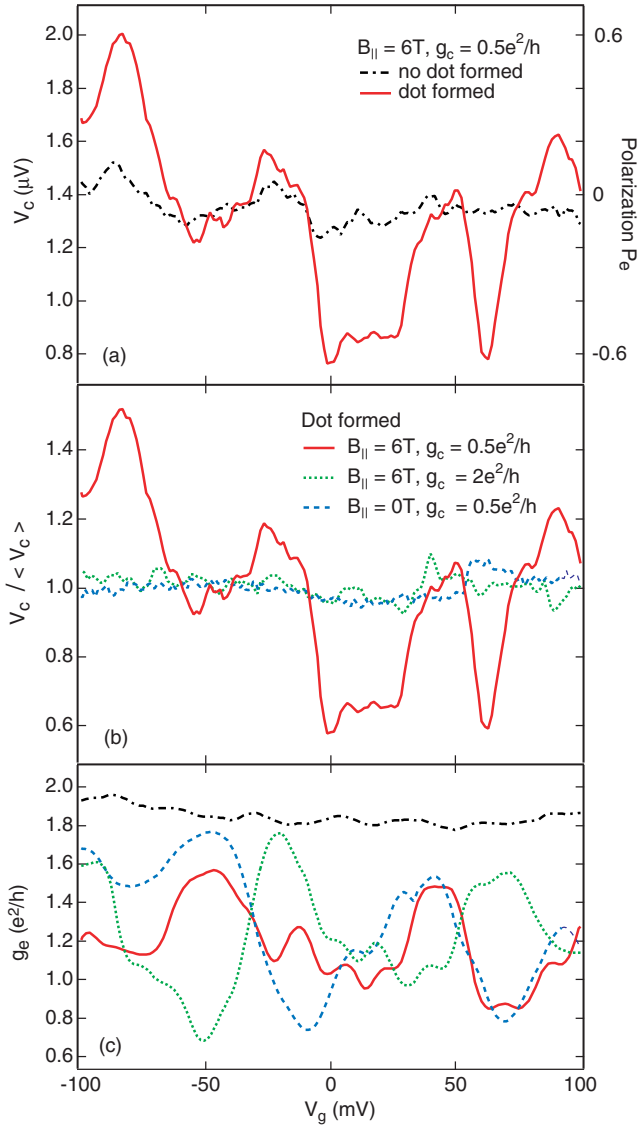

Figure 3.5: (a) Focusing peak height at $B_{\|} = 6T$ with spin-selective collector, $g_c = 0.5e^2/h$, comparing emitter as point contact at $2e^2/h$ (black curve), and emitter as quantum dot with both leads at $2e^2/h$ (red curve). With the unpolarized point contact emitter, focusing shows only weak fluctuations; with the quantum dot emitter focusing fluctuations are large, extending both above and below the unpolarized curve, demonstrating bipolar spin polarized current controlled by the gate voltage, V_g. (b) Comparison of normalized focusing peak height fluctuations as a function of V_g at $B_{\|} = 6\ T$ for a spin-selective collector, $g_c = 0.5e^2/h$, (red curve) and unpolarized collector $g_c = 2e^2/h$ (green curve). Focusing peak height at $B_{\|} = 0$ (blue curve) also shows only weak fluctuations. (c) shows conductance fluctuations for the four cases. The presence of conductance fluctuations even in the spin unpolarized cases, $P_c = 0$ (green), $P_e = 0$ (black), and $P_e = P_c = 0$ (blue), demonstrates that focusing fluctuations do not arise from conductance fluctuations.

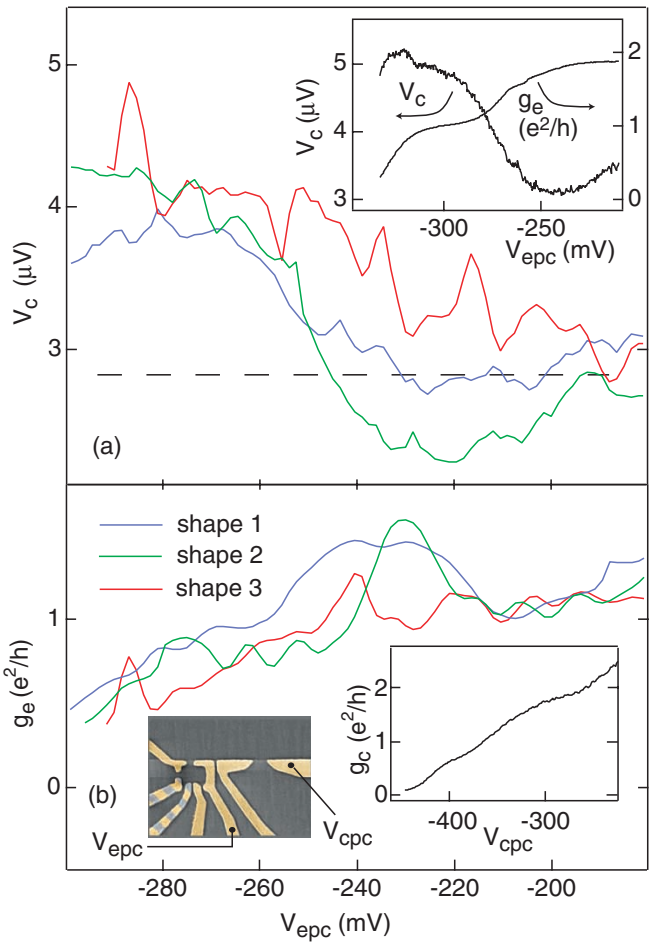

Figure 3.6: (a) Focusing peak heights at $B_{\|} = 6T$ for three different dot shapes as the exit point contact of the emitter dot is reduced from $2e^2/h$ (at $V_{epc} \sim -220\ mV$) to $\sim 1e^2/h$ (at $V_{epc} \sim -300\ mV$). The rising of the average focusing signal above the unpolarized level (dashed line) as the exit point contact is reduced below $2e^2/h$ demonstrates that spin currents of only a single polarization direction are possible when the exit point contact is spin selective. Inset: Emitter conductance, showing clear plateaus and corresponding focusing peak height when emitter is a single QPC. (b) Conductances of the emitter dot as the exit point contact is swept, for the three shapes shown above. Left inset: Micrograph indicating gates swept. Right inset: Collector point contact conductance, showing relatively weak plateaus.

will generate only a single direction of polarization, passing the lower energy spin, when the exit lead is set well below $2e^2/h$. A similar effect, where one direction of polarization becomes favored, is observed when either entrance or exit QPC, or both, is reduced into the tunneling regime. This complicates the use of Coulomb-blockaded quantum dots as bipolar spin filters, as is discussed in section 4.5.

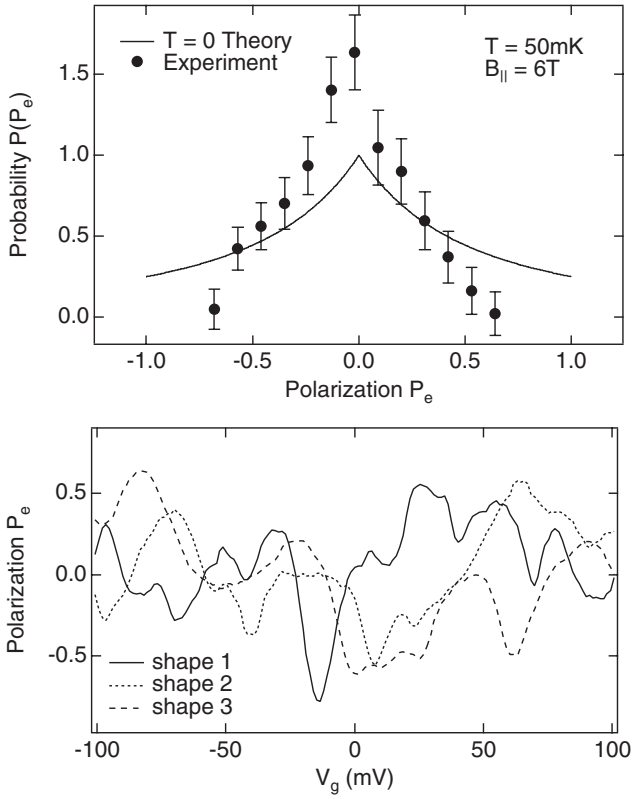

Figure 3.7: (a) Experimental distribution of emitter current polarization, P_e, over a dot-shape ensemble of ~ 200 independent samples, compared with random matrix theory (see text). Statistics for P_e are based on the value $P_c = 0.7$ extracted for this device (see text). (b) Examples of polarization fluctuations as a function of plunger gate, V_g for three different dot shapes.

Finally, in Fig. 3.7, we examine the statistics of the spin polarization of current emitted from the dot, sampled over an ensemble of dot shapes [38]. Roughly 200 independent shapes were used to generate the histogram shown in Fig. 3.7(a). For comparison, also shown in Fig. 3.7(a) is a simple random matrix theory calculation, treating the case of Zeeman energy greatly exceeding the dot level spacing, and for zero temperature and zero dephasing rate [53]. This model gives a probability density for the spin polarization of current of the form $P(p) = 1/(1+|p|)^2$, with zero average and typical fluctuations (standard

deviation) $\sigma(p) = 0.48$. Using the value of P_e determined above, the experimental value is $\sigma(p) = 0.27 \pm 0.06$.

It is not surprising that $\sigma(p)$ is overestimated by a zero-temperature theory. One may compare the reduction factor (relative to zero-temperature theory) for typical fluctuations of spin polarization to the analogous factor for conductance fluctuations. Conductance fluctuations measured simultaneously in the emitter dot gave $\sigma(g) = 0.21 \pm 0.02\ e^2/h$, which is 51% of the theoretical zero-temperature UCF value for single-mode leads [52], accounting for lifted spin degeneracy. This is consistent with the reduction factor $0.27/0.48 = 56\%$ observed for spin polarization. Note that, despite the reduction factor, spin polarizations up to $\sim 70\%$ are readily obtained.

3.4 Unexplained Features of the Focusing Signal

One of the most prominent features of our focusing data, and yet one which remains almost completely ununderstood, is the suppression of the first (and, to a lesser extent, the second) focusing peak at large fields, as seen in Figs. 3.1(c) and 3.1(d). This effect was observed over multiple cooldowns and for all point contact positions. Because the large fields used in this experiment were *in-plane* fields, one might expect that this feature is spin-related. We believe that this is not the case, however, first because the suppression occurs for all settings of the point contact—the effect is just as evident with the point contacts set on the $2e^2/h$ plateau, which is manifestly spin-degenerate as can be seen from the factor of 2, compared with when they are set to e^2/h or even below. If it were a spin effect one would expect that it would depend in a clear way on the polarization of electrons involved in the focusing process. Similarly, the values for polarization extracted from the first (and most strongly suppressed) focusing peak are similar to those extracted from the higher-order (and negligibly suppressed) focusing peaks. The polarization statistics presented in section 3.2 include all (first, second, and third) peaks.

Other effects which could cause a suppression in focusing peak height include increased scattering in the bulk 2DEG region. This appears not to be a correct explanation, at least in the simplest picture, because the scattering, monitored directly through measurements of the bulk 2DEG mobility, was not strongly influenced by the in-plane field. We note, however, that both the suppression of the first focusing peak and the quality of the focusing signal among all peaks (which tended to degrade substantially above roughly $B_{\|} = 2T$)

depended on the orientation of the in-plane field relative to the axis between the focusing point contacts.

Another effect that is not at this time well understood is that some focusing peaks undergo substantial shifts in perpendicular field as a function of in-plane field. Some shift is expected, due to distortions created by the in-plane field in the Fermi surface. However, the shifts observed in this experiment were substantially larger than the $\sim 10\%$ effect that would be expected from that effect. One experimental artifact that could also create the appearence of a field shift is that the perpendicular field felt by the sample was be slightly different than the applied perpendicular field, and was dependent on the "in-plane" magnetic field from the large external solenoid because there was a slight ($< 1^\circ$) misalignment of the sample plane with the axis of that magnet. However, we attempted to eliminate this effect by measuring the perpendicular field *on-chip* using a Hall bar fabricated on the same sample.

In addition, some of the focusing peaks appeared to *split* in in-plane field by substantially more than would be expected from the slightly different Fermi velocities of the two spin states in a large field. Such a splitting could not be explained by an error in our estimate of the local perpendicular magnetic field at the sample. In summary, there are several effects related to focusing in a $GaAs$ heterostructure in the presence of an in-plane field that bear further study.

Chapter 4

Spin Measurements in Coulomb Blockade

4.1 Introduction

The measurements described in Chapters 2 and 3 explore the spin physics of *open* systems—systems, including open quantum dots and quantum point contacts, that are well-coupled (through their leads) to the bulk. We now turn to an investigation of the spin physics of nearly-isolated or *closed* quantum dots. In such systems, the semi-classical approximation of quantum interference between different electron trajectories breaks down, and instead we consider transport through the wavefunctions which are the many-particle eigenstates of the dot.

Again, we turn to the question of whether the singlet-triplet exchange splitting is sufficient in these systems to create higher spin states. We investigate these questions by looking first at sequences of consecutive Coulomb blockade peaks (and thereby consecutive ground state transitions) to find if they alternate between spin-increasing and spin-decreasing transitions. Ground state spin states, for example, of 0, $\frac{1}{2}$, 0, $\frac{1}{2}$, 0, etc., would imply alternating increasing and decreasing transitions, whereas occasional ground states of spin 1 would imply deviations from a perfectly alternating pattern. The spin transitions themselves are determined by looking at changes in Coulomb blockade peak position as a function of in-plane magnetic field. As described in section 1.6.2, the peak position in gate voltage V_g may be expected to depend on ground state spin by the relation $eC_{gate}V_g/C_{dot} \sim (S_{N+1} - S_N)g\mu B$, and the spacings by $eC_{gate}\Delta V_g/C_{dot} \sim (S_{N+2} + S_N - 2 \times S_{N+1})g\mu B$.

In addition, we examine excited state spectra produced at a finite source-drain bias (which provides access also to excited spin states, whose energy above the ground state will then be influenced with a parallel magnetic field). This allows us to search, for example, for a splitting in spin 1/2 ground states at large in-plane fields relative to neighboring spin 0 states, whether those states are already split at zero field (for example by a spin-orbit interaction) [54], or to find if either spin-up or spin-down transitions are blocked by other effects.

There has been much discussion in the mesoscopics community of the possibility of using Zeeman splitting in the states of a Coulomb blockaded quantum dot to create a spin detector or spin polarizer [55]. It is generally expected that ground state spin transitions of different directions (spin 0 to spin 1/2, for example, or spin 1/2 to spin 0) would create spin detectors (or spin polarizers) of opposite sign. For example, in an in-plane field, where we will define the direction of the field to be "up", the ground state of an odd number of electrons N in a quantum dot may be spin 1/2, pointing up and thus aligned with the field (the negative sign of the g-factor in $GaAs$ is ignored here). The N+1 ground state might then be spin 0, and transitions between the N and N+1 ground states would involve transport of an electron *anti-aligned* with the external field. Similarly, if the ground state spins of the N and N+1 systems were reversed (spin 0 for the N electron ground state, where N would then clearly have to be even), transitions between the N and N+1 ground states would require transport of the spin *aligned* with the in-plane field. The thesis concludes, then, with a measurement of the the spin polarization of electrons engaged in transport as transitions between particular ground state spin states occur.

4.2 Ground State Spin Measurements

In this section we describe measurements of ground state (GS) spin for two quantum dots, one of area $\sim 0.2\mu m^2$ (Dot C) and the other of $\sim 0.1\mu m^2$ (Dot E), containing roughly 400 and 150 electrons, respectively. These dots were coupled to electron reservoirs via *tunnelling* leads (i.e., $g < 2e^2/h$ for both leads) so transport was dominated by CB effects. However, measurements are presented for two very different point contacts settings. For Dot C, data is shown both with the point contacts set to be weakly tunnelling (coupling to the leads was small, Coulomb blockade peak height $g_{max} \sim 0.05e^2/h$, escape rate $\Gamma_{esc} \sim \Delta/20$) *and* with them set to be strongly tunnelling, $\Gamma_{esc} \sim \Delta/3$. For Dot E data is presented only

for the point contacts set to be weakly tunnelling, $\Gamma_{esc} \sim \Delta/20$. These measurements were carried out at sufficiently low temperature and bias that the differences between N and $N+1$ electron GS energies were extractable from CB peak position, V_g.

To allow the applied field to couple predominantly to spin, the sample was oriented parallel to the field. For this measurement, it was especially critical that the perpendicular field remain constant. Whereas for the experiments discussed in Chapter 2, statistics were taken over mesoscopic fluctuations as a function of various parameters (and therefore deviations in perpendicular field should have no effect of the statistics), the peak position data presented in this section could only be trusted to represent *spin* effects as a function of in-plane field if the perpendicular field remained constant. To achieve the necessary alignment, the plane of the electron gas was first oriented along the axis of the primary solenoid and roughly aligned by hand to within 0.5 degrees of the axis of the primary solenoid. As mentioned in Section 1.3, the small pair of coils attached to the vacuum can of the fridge, oriented perpendicular to the plane of the sample, could then used both to break time-reversal symmetry explicitly, and to null out any perpendicular field that resulted from misalignment. Both the primary and trimming coils were under computer control, allowing sweeps of strictly parallel field to be made. (We estimate the uncertainty in $B_\perp$ to be less than $\phi_0/4$ through the dot at $B_\parallel = 5\,T$.)

Despite this precise field trimming capability, the measurements [1] in larger dots fabricated on the same wafer combined with parabolic motion of *all* peaks together indicated an orbital coupling even for the strictly parallel field (see section 2.2).

Conductance measurements across ten consecutive Coulomb blockade peaks, measured in Dot C as a function of V_g and $B_\parallel$ (i.e., *strictly* $B_\parallel$, properly trimmed) are shown in Fig. 4.1. More positive gate voltage corresponds to higher energy, and can be calibrated exactly using high source-drain bias measurements. All data were taken with the perpendicular component of the field held constant at $20mT$ in order to ensure that time-reversal symmetry was broken and GUE statistics would apply. In addition to the individual motions of each peak, there is a diamagnetic shift common to all peaks, shown in Fig. 4.1(b) as the average over all peak positions. In subsequent data sets, this common curve is subtracted from each peak position; it was presumably due to the effect of the parallel field on the effective well confinement potential. The slight paramagnetic shift visible at low field ($B_\parallel < 0.2T$) may have been due to magnetic materials in the low temperature filters for the signal wires, or to ferromagnetism in the ohmic contacts ($NiAuGe$) that were used for this device.

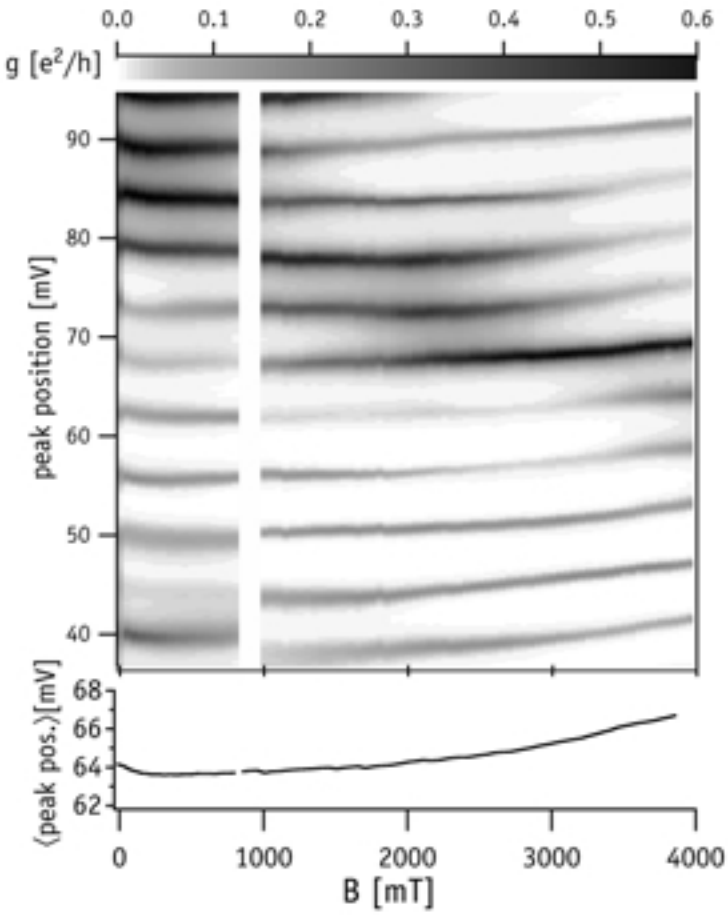

Figure 4.1: (a) Coulomb blockade peaks measured for Dot A ($0.25\mu m^2$), with the point contacts set to be strongly tunnelling (coupling to the leads is strong), as a function of in-plane magnetic field. A diamagnetic shift in the peak position, common to all peaks, is clearly visible. The *average* peak position (averaged over all 10 peaks), reflecting only this parabolic motion, is shown in (b). The paramagnetic shift at low in-plane field $B_{\|} < 200mT$ is not well understood (see text).

Peak positions and peak spacings extracted from the peaks in Fig. 4.1 are shown in Figs. 4.2 and 4.3. The slope of peak positions in Fig. 4.2 as a function of $B_{\|}$ is consistent with a Zeeman energy term $E_S = \pm\frac{1}{2}g\mu_B B$, using the g-factor for bulk $GaAs$, $|g| = 0.44$. As discussed in the Introduction, alternating slopes for consecutive peaks would indicate an alternating $0, \frac{1}{2}, 0, \frac{1}{2}...$ GS spin structure. Our data, on the other hand, shows three consecutive pairs of peaks moving with the *same* slope, suggesting the presence of higher spin states. Proposed values for the nine consecutive GS spin states shown here are included

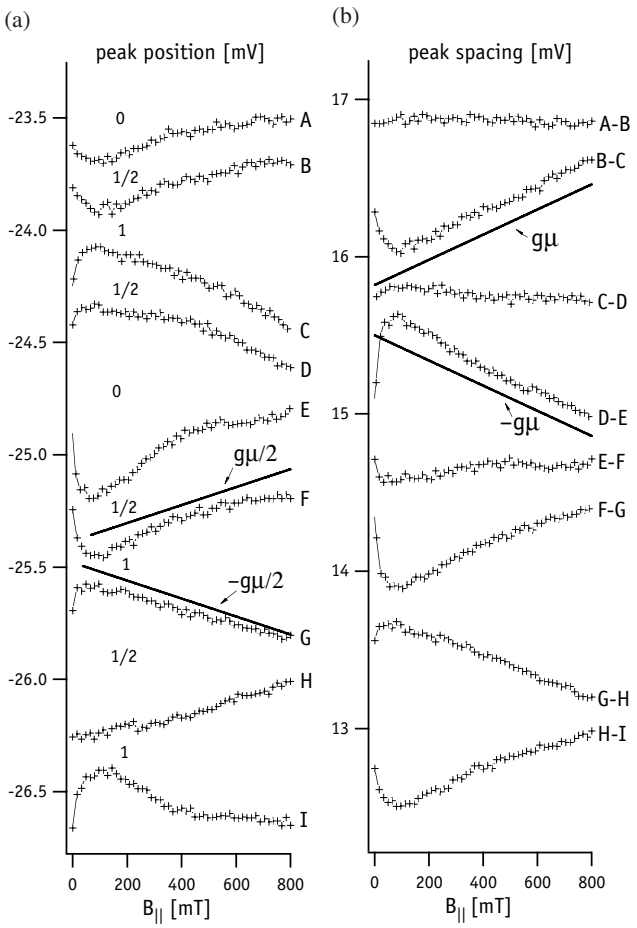

Figure 4.2: Peak positions (a) and spacings (b) extracted from the low in-plane field data shown in Fig. 4.1. Motions are consistent with $E_S = \pm\frac{1}{2}g\mu_B B$ for the peak positions and $E_S = 0, \pm g\mu_B B$ for the spacings as expected. The diamagnetic shift extracted in Fig 4.1(b) is removed from all data shown here.

in Fig. 4.2(a). We emphasize, however, that these are only plausible values for the spin; it is not possible to determine unambiguously the absolute magnitude of GS spin from measurements of peak position, which reflect only *changes* in spin from the N to N+1 ground states. The values shown in Fig. 4.2(a) minimize the ground state spin for the system (assuming this to be a positive number). In the proposed spin labelling scheme, three out of the five even-N states have $S = 1$, i.e., $P(S = 1) \sim 0.6$.

Figure 4.3 shows that peak spacings clearly separate into three branches, a top branch with slope roughly $g\mu$ (corresponding to a GS spin decrement followed by an increment) a bottom branch with slope roughly $-g\mu$ (corresponding to a GS spin increment followed by a decrement) and a middle branch with slope near zero (corresponding to two consecutive

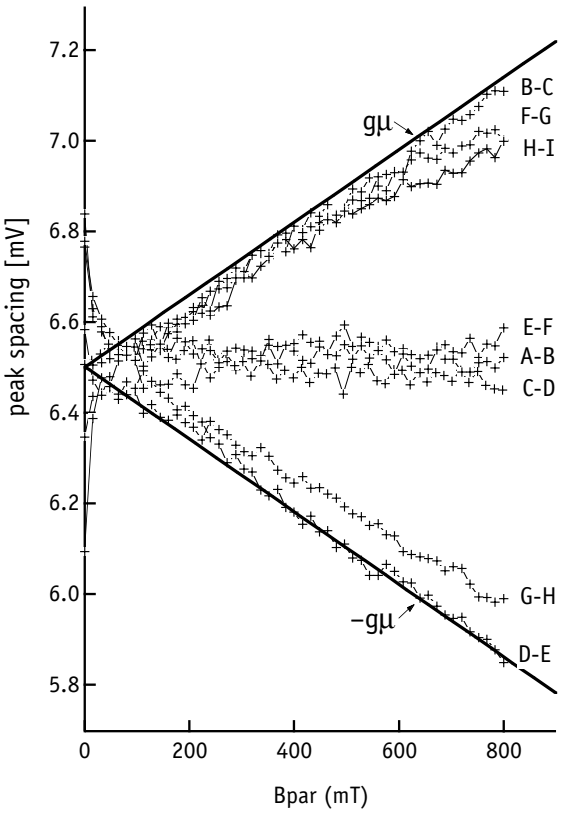

Figure 4.3: Peak spacings shown in Fig./ 4.2, offset to show grouping of slopes as $E_S = 0, \pm g\mu_B B$ for the spacings as expected. Continuation of linear behavior down to low fields, $g\mu B < kT$, is not well understood.

increments or decrements). The existence of the middle branch is the signature of higher GS spins. The good agreement between the slopes of the upper and lower branches and the expected slopes of $\pm g\mu$, as well as the absence of a range of intermediate slopes suggest that the peak spacing reflects spin rather than orbital coupling.

At higher fields, the directions of peak motion change, often abruptly and from one straight segment to another, as seen in Fig. 4.4. This behavior is qualitatively similar to numerical data presented in Ref. [2]. The rounding of straight segments where the slope changes may result from spin-orbit interaction which mixes spins, and may provide a direct measure of spin-orbit interactions in dots.

It is interesting to remember that the peaks analyzed in Figs. 4.1 through 4.4 were measured in a regime of high tunneling conduction in the leads. This can be seen clearly by noting the grayscale of Fig. 4.1. When the dot is more pinched off from the reservoirs, so that the CB peaks have a height of $0.1e^2/h$ or less, peak motion in this device was more

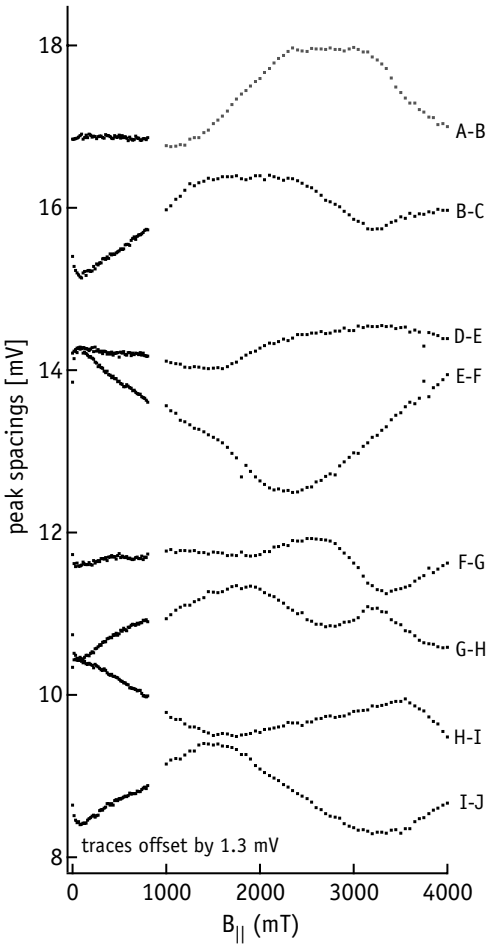

Figure 4.4: Peak spacings for the same peaks shown in Fig. 4.1, for high in-plane field ranges.

difficult to interpret, and at times did not seem to follow the clear patterns illustrated, for instance, in Fig. 4.4—certainly there appeared to be more "rounding" in between the linear segments. However, the clear spin dependence observed for the more open point contacts may be found in the more isolated regime as well.

One interesting feature of Figs. 4.2-4.3 is that the linear behavior of peak motion appears to continue down to very low in-plane fields ($< 100mT$). This is much smaller than field that one might expect from a comparison of Zeeman energies to thermal broadening: $g\mu B = kT$ at 200mT for the temperature of $\sim 60mK$ at which this experiment was performed, and thermal broadening in the leads is expected to be $3.5kT = g\mu B$ for B=$700mT$. This effect is not well understood. In contrast, the flat peak motions with the dot more nearly isolated

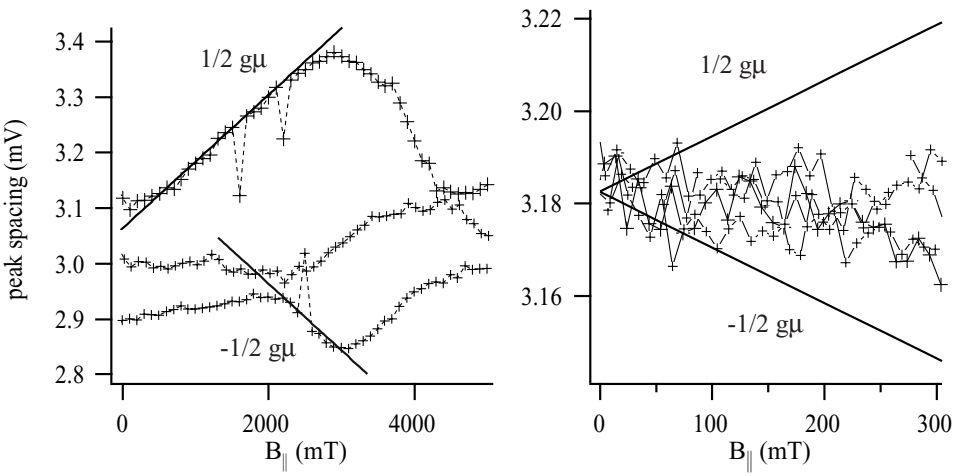

Figure 4.5: Peak spacings for four consecutive peaks for Dot C, now with point contacts set to provide weak coupling to the leads. (a) Slopes of $\pm\frac{1}{2}g\mu$ are still apparent, though not as clearly visible as in the open regime. (b) At low field the slopes of all peak motions appear to be nearly zero (see text).

(see in Fig. 4.5(b)) are easily understood as simply the effect of thermal broadening. We do not have an explanation for the different behavior depending on whether the dot is more closed or more nearly open.

From Dot C, Figs. 4.1-4.5, we can see that peak motion in an in-plane magnetic field reflects ground state spin energies. However, the fact that the behavior was more clear in what would otherwise be considered a more complicated regime—when the dot was strongly coupled to the leads—is surprising and makes simple interpretation of the results more difficult.

When a dot is *weakly* coupled to the leads, it may better be considered as an isolated object having well defined ground state spins, with the leads only a small perterbation. A clearer example of the spin dependence of peak motion with a nearly-isolated dot was observed in Dot E. The peaks investigated in this device, together with the spacings extracted from them, are shown in Fig. 4.6. One reason that the spin signatures from this dot are more clear may be that the dot is smaller by a factor of three. Again, the presence of flat spacings (spacings which do not change as a function of in-plane field) indicates higher spin states, and a possible enumeration of spin states is also shown.

The appearance of these higher spin ground states, such as the triplet state S=1, in both quantum dots measured implies that the effect on this system of an exchange interaction, J, can not be neglected. In the absence of such an interaction, if one begins with an odd

number of electrons in the dot (spin 1/2), it would be energetically more favorable to put an additional electron into the same orbital as the unpaired spin, creating a singlet state and returning the dot to spin 0. To create the S=1 triplet state would imply putting the additional electron the *next* orbital, thereby costing an orbital level spacing Δ in energy. However, the presence of an exchange interaction J can reduce the singlet-triplet splitting $E_{triplet} - E_{singlet}$ below Δ and even below zero, making the triplet the ground state for the system.

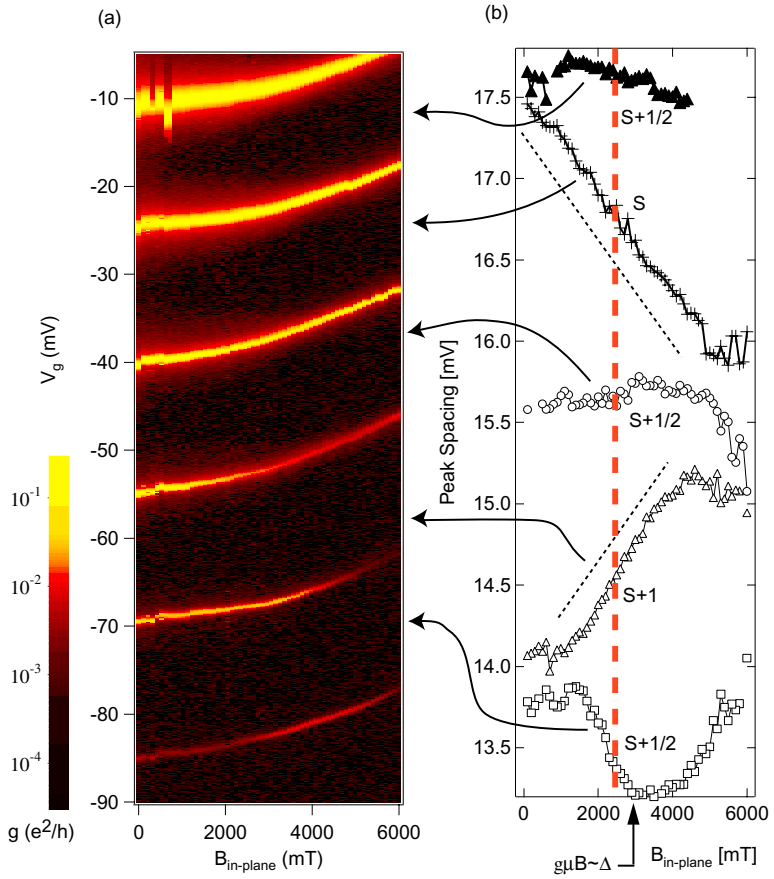

Figure 4.6: (a) Coulomb blockade peaks in Dot E, observed as a function of in-plane field in the nearly-isolated regime. Note that, compared with Fig. 4.1, the peaks are narrower and have lower conductance. (b) Peak spacings for the five consecutive peaks shown in Fig. 4.6, showing clear motion with in-plane field with slopes of $0, \pm g\mu$. At a field of $2.5T$, indicated by the dashed orange line, a possible listing of ground state spins is shown (with S an arbitrary half-integer but probably close to zero). Note, each spacing curve has associated with it a particular ground state spin, since the spin is (in principle) well-defined in each Coulomb valley where the number of electrons is fixed. This should not be taken to indicate that the particular dependence of a given peak spacing, by itself, on in-plane field in some way determines the precise ground state spin for that Coulomb valley, see Eq. (1.2).

Random Matrix Theory allows the probability of S=1 ground states to be calculated as a function of J (assuming broken time reversal symmetry) [2, 54]. The calculations in Ref. [2] indicate that the appearance of S=1 ground states with a probability $P(S = 1) = 0.6$ implies an exchange energy $J \sim 0.6\Delta$ at zero field, although for improved estimate of the value of J in this system it would be necessary to collect more statistics.

4.3 Orbital Effects of a Parallel Field

Despite precise trimming out of any perpendicular component from an "in-plane" field due to misalignment of the sample and field axis, there are always orbital effects from an in-plane field. These apparently result from a combination of several effects. First, as mentioned before there is a diamagnetic shift common to all Coulomb blockade peaks, which is presumably due to changes in the effective confinement potential in the growth direction of the heterostructure resulting from the applied field. Second, there appears to be some coupling to the orbital wavefunction itself, due either to "roughness" in the 2DEG (deviations from a perfect plane) or asymmetry in the heterostructure. Finally, there will be an orbital effect of any spin splitting to the extent that a spin-orbit interaction is present in the system. These effects are still being further studied at the writing of this thesis, for example in Ref. [33].

The result of this orbital coupling even from a strictly in-plane field is that it is not, in fact, appropriate to assume that *only* the Zeeman energy is affected as the in-plane field is changed. This means that one must be careful to distinguish peak motion in an in-plane field that is due to Zeeman shifts in the ground state spin energy from, for example, shifts in the orbital energy level splittings Δ, which could in principle show mesoscopic fluctuations as a function of in-plane field. Generally, for work done in this thesis, we have found motions (both in ground and excited states) that are both linear and with slope corresponding to $g\mu$; these we have interpreted as due to spin energies and not orbital coupling. As a warning to the reader, however, this may not be in every case the correct interpretation. In many cases we draw conclusions about the spin physics of the dot from the fact that some features of the peak motion do not appear to follow a simple spin picture. Of course, if the peak motions under study were not reflecting changes in spin energies, but rather changes in orbital energies, then these conclusions would be incorrect.

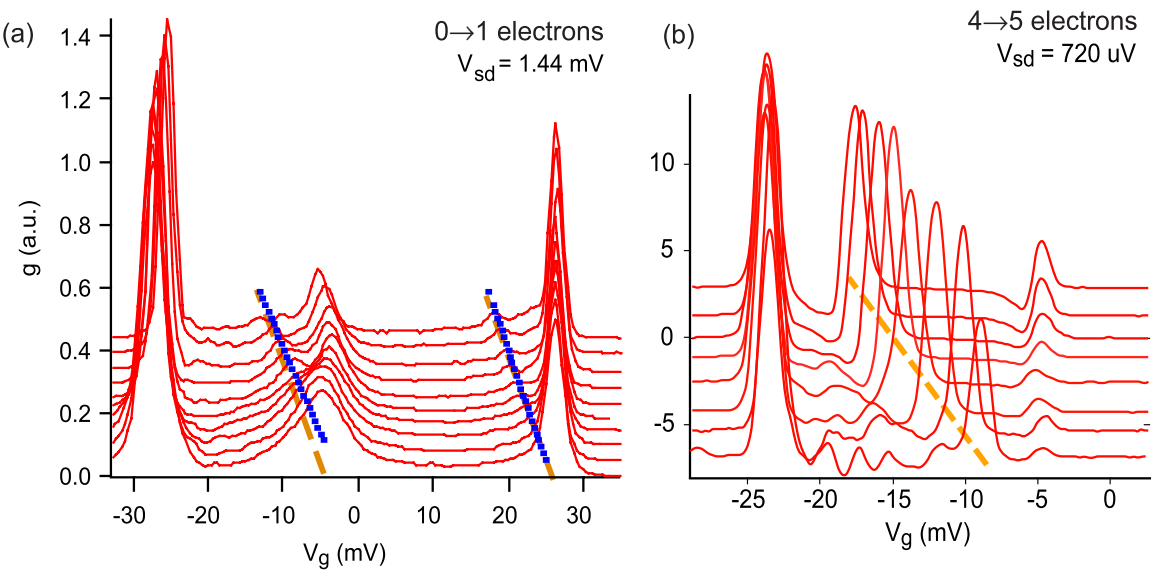

Figure 4.7: Excited states measured for a few-electron dot as a function of in-plane magnetic field, from $B_{\|} = 0$ (bottom trace in (a) and (b)) to $B_{\|} = 9T$ (top traces). Yellow dashed lines represent slopes of $g\mu$ relative to the ground state. In both traces, the ground states are aligned in gate voltage by hand for all fields. (a) Splitting is observed for the $0 \rightarrow 1$ electron ground state transition (shown here with an applied bias of $V_{sd} = 1.44mV$), reflecting the difference in energy to add a spin-up or spin-down electron to the first orbital state in the dot. Similarly, a splitting appears in the excited state peak, probably corresponding to the electron entering the second orbital state in the dot. (b) No such splitting is observed for the ground or excited $4 \rightarrow 5$ electron transitions (shown here with an applied bias of $V_{sd} = 0.72mV$). Nevertheless, the excited state is observed to decrease in energy relative to the ground state with slope approximately $g\mu$ (dashed yellow line), suggesting that the ground and excited states represent different spin transitions.

4.4 Excited State Spin Measurements

As mentioned in the introduction, it should also be possible to observe spin physics, and particularly spin splittings, in excited state spectra measured at a finite source-drain bias. Ground and excited state spin splittings have been clearly observed in nanotube dots, for example, in Ref. [19]. In $GaAs$ quantum dots, however, such a simple picture has never been found.

One expects to see spin splitting in the ground state as the N+1 level passes the source, for N even, and as the N+1 level passes the drain, for N odd. Excited states should show a splitting in all cases. In one case, we believe that we have observed this behavior. This was in an extremely small dot formed following the work of Ref. [56] (Dot D, see Fig. 4.7(a)). The splitting was observed for the Coulomb blockade peak corresponding to the transition between 0 and 1 electrons in the dot. For this transition splittings were observed in the

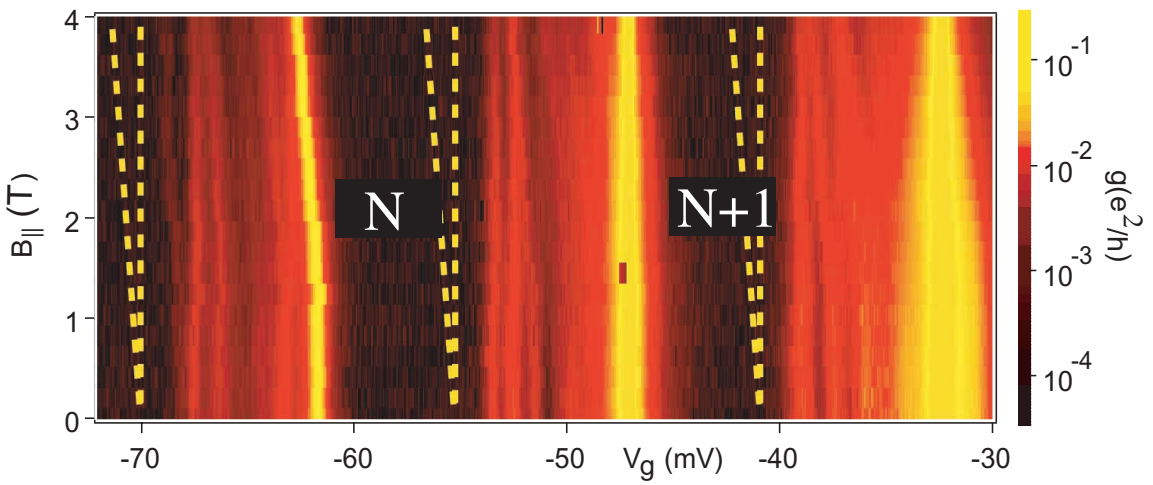

Figure 4.8: Excited states measured as a function of an applied parallel field in the emitter dot of the focusing device, using $V_{sd} = 500\mu V$ dc bias. The traces are shifted such that the $N+1 \rightarrow N+2$ electron transition (following the notation in this figure) occurs at $V_g = -32.5mV$ (ground state passes drain). Yellow dotted lines correspond to energy splittings of $g\mu B$, as expected for Zeeman splittings (using the g-factor $g = -0.44$ for bulk $GaAs$). Some excited states clearly show level motion following Zeeman energies (parallel to the yellow dashed lines) but only in the case of the $N-1 \rightarrow N$ ground state passing the source (at $V_g = -69mV$) is a clear zero-field spin degeneracy (and subsequent spin splitting) observed.

ground state as well as in the only excited state accessed in the measurement. The splittings appear to have the "appropriate" slope, $g\mu$, and to extrapolate to zero at low field.

Even for the next Coulomb blockade peak, presumably accessing the 1 to 2 electron transition, the story is not nearly so simple, and in general splittings are only occasionally observed in either ground or excited states (see Fig. 4.7(b)). In the $4 \rightarrow 5$ electron transition shown here, neither the ground state nor the excited state appears to split, but the excited state moves with slope $g\mu$ relative to the ground state, suggesting, for example, that the excited state is a higher spin state (spin 1?) than the ground state (spin 0?). However, we note that this explanation of the data is not fully consistent, because it does not explain the lack of splitting (3-way, for a triplet) observed in the two states. Furthermore, the difference in tunnel coupling for the two spin directions should be visible in the relative heights of the ground and excited states, but as a general rule no such correlation is observed.

When excited state spectra were observed in many-electron dots, such as Dot E, no consistent splitting was observed. An example of such an excited state spectrum is shown in Fig. 4.8. Clearly, some levels move with slopes corresponding to $g\mu$ (relative to others) as expected, but in only a few cases is a clear splitting (originating at zero field) observed. Again, there appears to be no correlation between the direction of movement in field for a

state and its relative peak height.

We do not have a good explanation for the lack of splitting observed in many-electron quantum dots in both ground and excited states. Indeed, conversations with others in the quantum dot community suggest that the failure to observed consistent spin splittings is a common feature of $GaAs$ quantum dot transport, and will require further study to be understood.

4.5 Spin Polarization of Transport Current

As described in the Introduction, one would expect a correlation between the direction of ground state spin transition (increasing or decreasing) for a given Coulomb blockade peak and the spin of the electrons participating in transport on that peak.[55] It was this correlation that we hoped to observe using devices such as that shown in Fig. 1.2(e), which shows Dot E built into a focusing configuration. As was discussed in section 1.6.3, the focusing signal from such a device obeys Eq. (1.2), and thus from measurements of the focusing signal the polarization of the electrons involved in transport may in principle be observed. In this section, therefore, we extend the same type of measurements presented in Chapter 3 to measurements of the spin polarization of currents on Coulomb blockade peaks.

Before doing so it was necessary to demonstrate that a transverse focusing measurement from an emitter in the Coulomb blockade regime was even possible. To our knowledge these types of measurements had never been done before this work. There were two clear difficulties: first, the measurements presented in Chapter 3 were all performed with a constant current through the emitter (a current bias). Thus the current I_e included in Eq. (1.2) was held fixed, and the collector voltage served as a direct measure of polarization. Of course, it is not possible to maintain a constant current in the Coulomb blockade regime, where the conductance often drops to nearly zero and thus an extremely large voltage would be dropped across the device. Instead, a constant emitter voltage is maintained, and the current, I_e—which is measured independently—is divided out to provide information about polarization. As shown in Fig. 4.9, we first confirmed that this worked in the *open* dot regime. We tried an open dot measurement as presented in Chapter 3 first with a constant current and then again with a constant emitter voltage, and compared the polarizations obtained in each case. As can be seen in Fig. 4.10, the two agree very well.

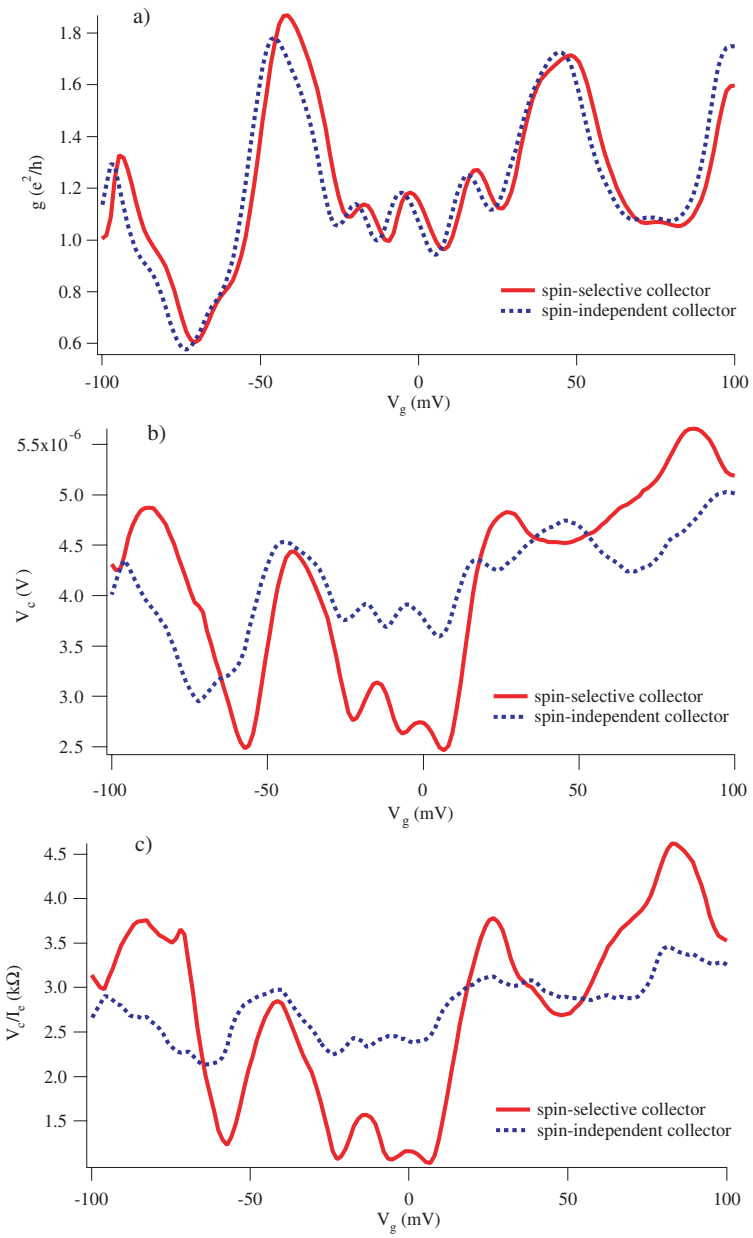

Figure 4.9: Measurements on the open dot described in Chapter 3 (Dot E), applying now a constant *voltage* rather than a constant current across the emitter and measuring the resulting current through the emitter. (a) Emitter conductance, g_e, showing fluctuations as in Fig. 3.4. A constant resistance is subtracted off to account for lead resistance. (b) Collector voltage, V_c, monitored simultaneously with the conductance shown in (a) for an unpolarized ($g_c = 2e^2/h$, blue) and polarized ($g_c = 0.5e^2/h$, red) collector point contact ($B_\parallel = 6T$). (c) Collector voltage normalized by emitter conductance, V_c/I_e, showing that fluctuations remain for the case of a polarized collector, but disappear with unpolarized collector.

The current from an emitter in the Coulomb blockade regime is necessarily small, as the

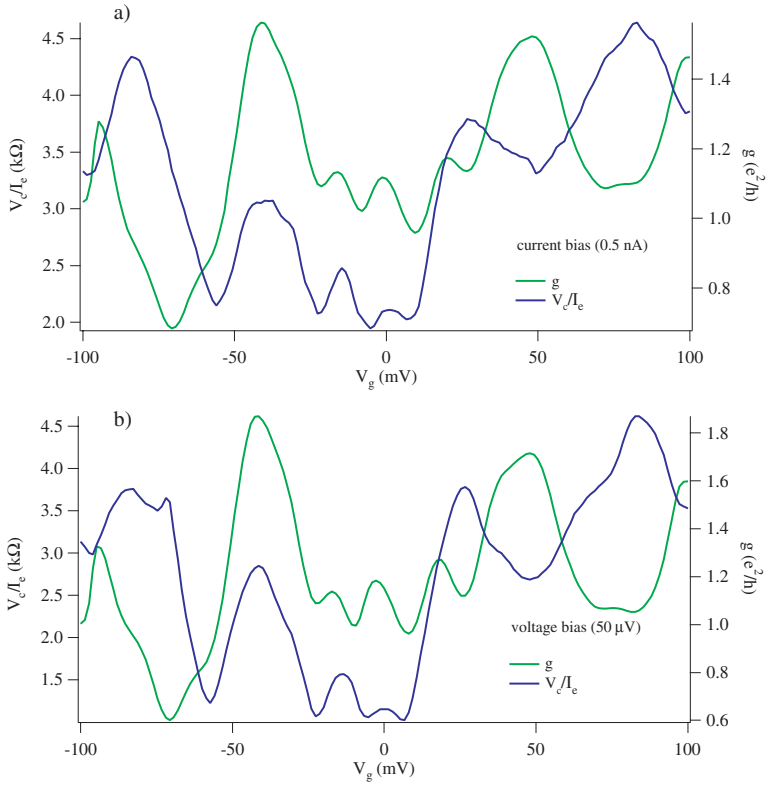

Figure 4.10: Comparison of the conductance and focusing signal for (a) current bias and (b) voltage bias configurations. Note the similarity of the two measurements, indicating that the measurement configuration used does not affect the results. The collector voltage is normalized by emitter current in order account for fluctuations in emitter current.

conductance $g_e \ll e^2/h$ (large voltage biases across the source and drain are undesirable if ground state properties are to be observed). This leads to the difficulty of detecting the focusing signal out of background voltage noise. We found that, using lock-in measurements at $\sim 17Hz$ and a lock-in time constant of $1s$, the voltage noise across the collector could be kept to $\sigma_v < 10nV$. With a typical collector conductance of e^2/h, a coupling "efficiency" of $\alpha \sim 0.25$ (the fraction of emitter current that actually enters the collector at the focusing condition), and an emitter voltage bias of $5\mu V$, this translated to an effective emitter conductance noise of $\sigma_g = \frac{e^2}{h}\frac{\sigma_v}{\alpha V_{sd}} \sim 0.01e^2/h$. For the measurements involving lowest emitter conductance, this then required multiple traces (10-50) over identical parameters to reduce noise to an acceptable level.

With these concerns taken into account, we tested whether focusing could be successfully observed in Coulomb blockade, as shown in Fig. 4.11. This figure shows a Coulomb blockade

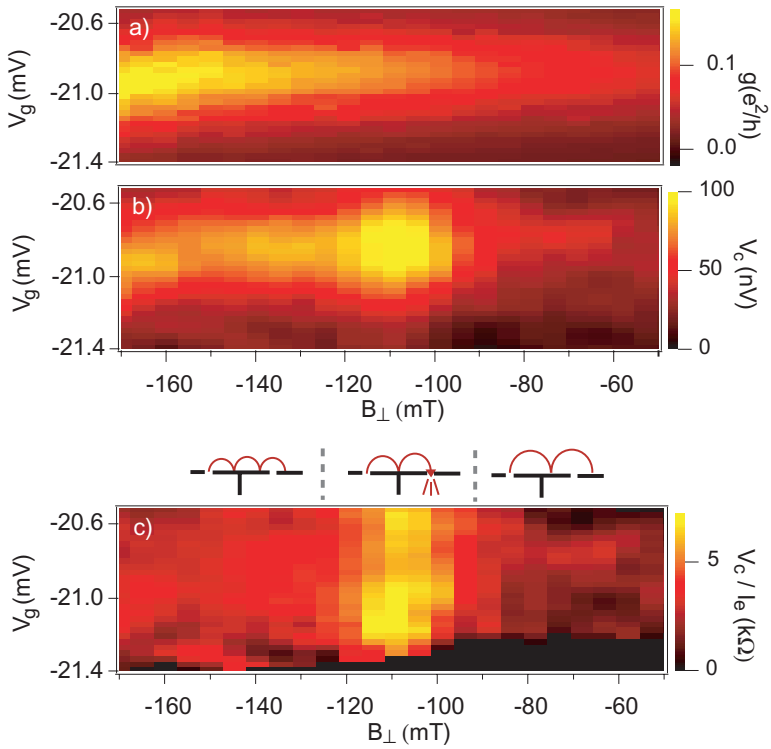

Figure 4.11: Here, the emitter dot is put into the Coulomb blockade regime and both the emitter conductance and collector voltage are measured as a function of gate voltage and perpendicular magnetic field. (a) The emitter conductance, g_e, shows the Coulomb blockade peak changing in height and position as a function of perpendicular magnetic field. (b) The collector voltage, V_c, measured simultaneously, showing the focusing signal at $-110mT$. (c) The focusing signal becomes much clearer when the ratio V_c/I_e is plotted instead, with consideration taken for differing time constants on the lock-ins measuring conductance and collector voltage (see text).

peak observed as a function of perpendicular magnetic field; fluctuations in the height and gate voltage position of the conductance peak reflect changes in the orbital wavefunction in the dot. The collector voltage, measured simultaneously, is shown in Fig. 4.11(b). The collector voltage drops when either the current through the emitter drops or the focusing condition is not met. To account for changes in the emitter current, we show the collector voltage divided by emitter current, V_c/I_e, in Fig. 4.11(c).

One subtlety of this calculation, unfortunately discovered only after the data was taken, is that the lock-in time constants were different for the emitter conductance and collector voltage measurements—the time constant on the conductance lock-in was kept at $100ms$, much less than the ~ 0.7 seconds delay in between data points, but the collector lock-in used a time-constant of $1s$ to reduce noise. Therefore, in Fig. 4.11(c) the emitter conductance

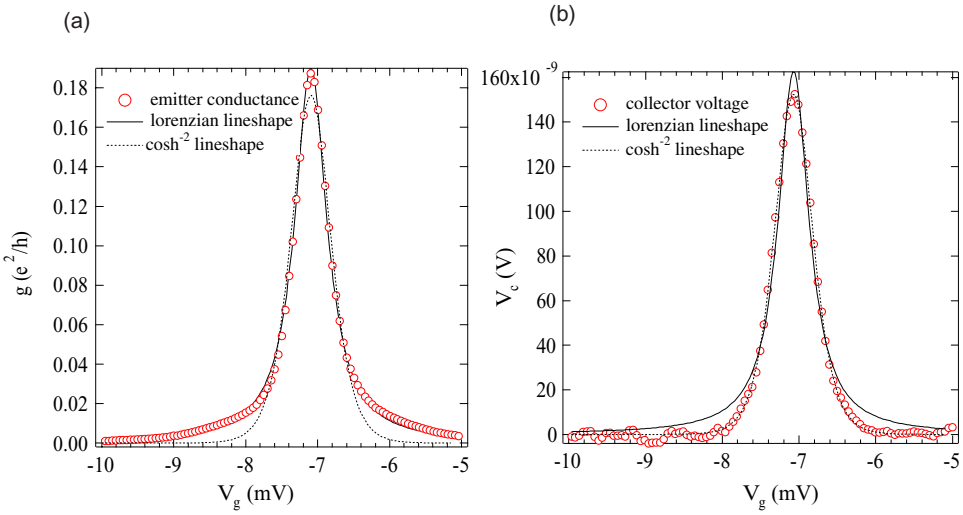

Figure 4.12: At $B_{\|} = 4T$, comparison of the Coulomb blockade peak shape for (a) conductance and (b) focusing signal. The conductance trace shows a closer fit to a lorenzian lineshape, probably due to escape broadening, while the focusing trace shows a closer fit to a $cosh^{-2}$ lineshape.

(and therefore emitter current I_e) is convolved with the step function response of the lock-in output filter at $1s$ before the division V_c/I_e was performed. As can be observed from the image of V_c/I_e, there is a dramatic peak in the focusing signal at the focusing condition, even in the Coulomb blockade regime.

The measured collector voltage and emitter conductance over a single Coulomb blockade peak at the focusing condition (and at $B_{\|} = 4T$) are shown in more detail in Fig. 4.12. The collector voltage is nearly proportional to the emitter current as expected from Eq. 1.2, with one surprising exception. As can be seen from Fig. 4.12(a), the conductance of the Coulomb blockade peak shown has a much closer fit to a lorenzian, compared to the $cosh^{-2}$ lineshape that would result from thermal broadening. This implies that the emitter current (from which the conductance was extracted) also followed a lorenzian dependence on gate voltage. Nevertheless, the collector voltage has instead a much closer fit to the $cosh^{-2}$ lineshape as seen in Fig. 4.12(b). This lack of proportionality between emitter current and and collector voltage remains unexplained at this point. Note that whereas peak positions depend on whether the the step function convolution described in the previous paragraph is taken into account, these peak shapes depend only negligibly on this effect.

Returning to the initial goal of the measurements of emitted current spin polarizations,

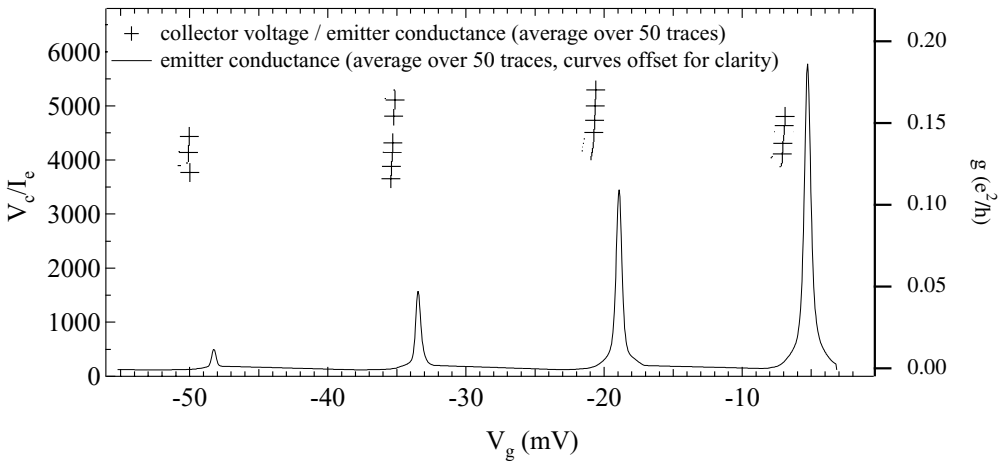

Figure 4.13: Emitter conductance for four Coulomb blockade peaks (peaks 3-6 in Fig. 4.6) at $B_{\|} = 4T$. Focusing signal for these peaks is shown as the ratio V_c/I_e, which should give a direct measure of spin polarization. Despite the fact that, based on data shown in Fig. 4.6, the spin transitions are opposite for peaks 4 and 5, there is only a slight change in the focusing signal (when normalized by I_e) between the two peaks (measured with the collector point contact at $0.5e^2/h$).

we compared the focusing signal for spin increasing and spin decreasing transitions. These measurements were taken on the same device, during the same cooldown, as the measurements of ground state spin transitions via Coulomb blockade peak motion presented in Fig. 4.6; the focusing measurements were all performed at $B_{\|} = 4T$. Indeed, the Coulomb blockade peaks used here were the same as those shown in Fig. 4.6. Therefore, we may compare the implications from the ground state spin transitions shown in Fig. 4.6 to the spin of the emitted current on the peaks measured directly. (Focusing data from only four peaks are shown here, as the focusing signal for the lowest conductance peaks was obscured by noise. Note that, even for these data, 50 traces were averaged together.)

We find no correlation between the ground state spin transitions extracted from Fig. 4.6 and the spin polarization of emitted current extracted from Fig. 4.13. Indeed, despite the fact that Fig. 4.6 implies that spin transitions of both directions are occuring in this system, the polarization of emitted current appears not to fluctuate. (We attribute small changes in the focusing signal to small changes in the coupling efficiency between emitter and collector at the focusing field.)

A similar effect may be observed by measuring the focusing signal for excited state spectra, also taken at $B_{\|} = 4T$ (see Fig. 4.14). Although more data would be needed for

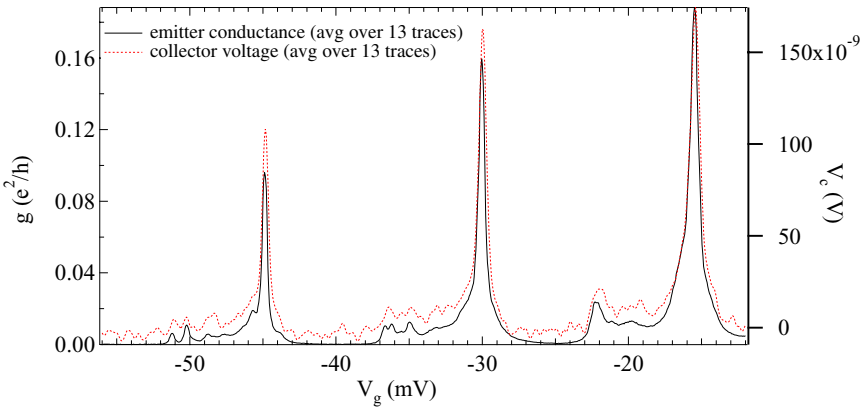

Figure 4.14: Emitter conductance and focusing signal for the three largest Coulomb blockade peaks shown in the previous figure (peaks 4-6 in Fig. 4.6 at $B_{\|} = 4T$, collector point contact at $0.5e^2/h$). Despite prominent noise in the focusing data, it is possible to note the conductance features (representing different excited states) mimiced proportionally in the focusing signal. This indicates that the features visible here were all of the same spin.

a more definitive statement, most of the features in the excited state conductance seem to produce a proportional collector voltage at the focusing condition, suggesting that the spin polarization of emitted current is the same for all features observed in the conductance measurements. This again is surprising, given that in Fig. 4.7 some states were seen to move at slope $g\mu$ relative to others.

One possible explanation for the lack of fluctuations in spin direction (for the emitted current) is that the dot point contacts are serving not only as tunnel barriers, but spin-selective tunnel barriers. This is not surprising given the results discussed in Chapter 3. There it is found that the spin polarization of current emitted through a point contact in a large in-plane field increases to some limiting value as the point contact falls deeper into the tunnelling regime, suggesting that the tunnel rates for spin-up and spin-down electrons remain dramatically different even in a tunnelling point contact. Any requirement for the spin polarization in the transport electrons due to ground state spin transitions would then have to compete with the difference in tunnel rates for the two spins. Indeed, in section 3.3 it was observed that the fluctuations in the spin polarization of emitted current from a dot disappear when one changes one of the point contacts from an open to a tunnelling regime.

This scenario is supported by the data presented in Fig. 4.15. Again, no fluctuations in the focusing signal are observed once the emitter dot is in the tunnelling regime (below

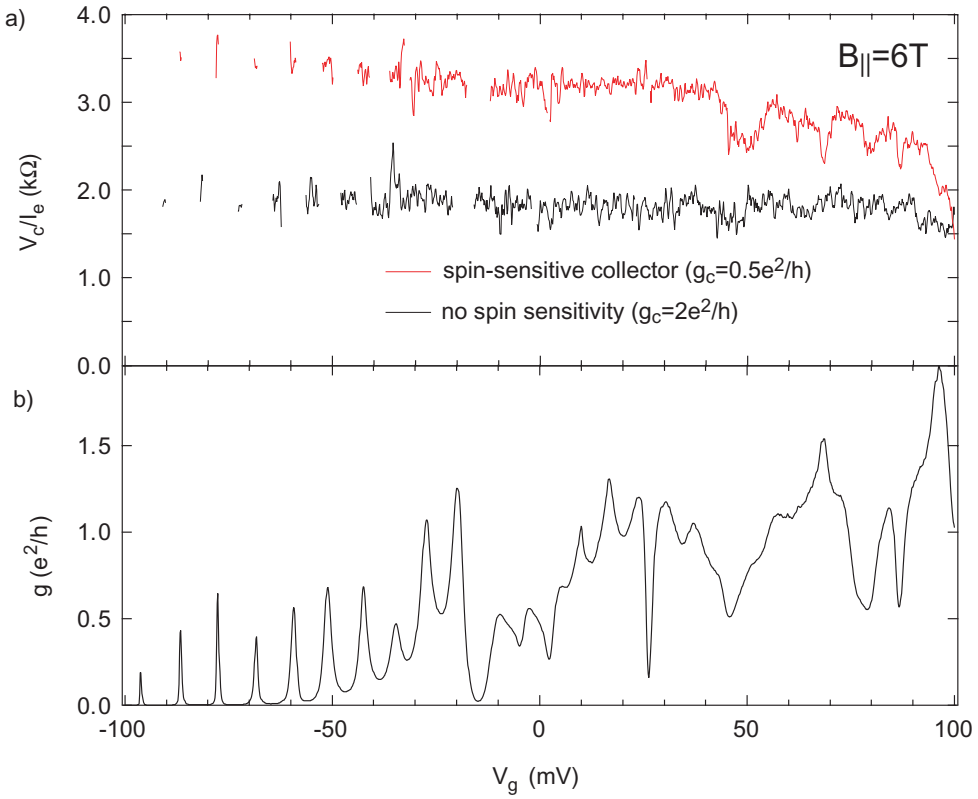

Figure 4.15: (a) Focusing signal at $B_{\|} = 6T$ from Dot E, with spin-selective ($g_c = 0.5e^2/h$, red curve) and spin-independent ($g_c = 2e^2/h$, black curve) collector. The polarization of current fluctuates on a typical gate voltage scale of $V_g = 5mV$, but these fluctuations are suppressed as V_g is reduced below $30mV$. At the same time, the spin selective curve rises to nearly twice the value as the curve at $g_c = 2e^2/h$, as would be expected from Eq. (1.2) if the emitter current were all polarized in the direction of the field (as from a tunnelling point contact). (b) Conductance measured simultaneously with data in (a).

$V_g \sim 30mV$). In addition, the focusing signal observed with the collector at $2e^2/h$ (expressed as V_c/I_e) is nearly twice the signal with the collector at $0.5e^2/h$. From Eq. (1.2), this suggests that the polarization of the emitted current is constant, and in the same direction as would be found for a single tunneling point contact.

One surprising aspect of this explanation, of course, is that the competition referred to above between the polarization required by energetically-allowed spin transitions and the dramatically different tunnel rates for the two spin should lead to a strong correlation between Coulomb blockade peak height and ground-state spin transition. Such a correlation is not observed. In general, a thorough theoretical explanation of the spin polarization of

emitted current through nearly isolated quantum dots in the presence of spin-dependent tunnel barriers will require further study.

Bibliography

[1] J. A. Folk *et al.*, Phys. Rev. Lett. **86**, 2102 (2001).

[2] J. A. Folk *et al.*, Physica Scripta **T90**, 26 (2001).

[3] A. G. Huibers, *Electron Transport and Dephasing in Semiconductor Quantum Dots*, Ph.D. thesis, Stanford University (1999).

[4] S. R. Patel, *Electronic Ground State Properties of Coulomb Blockaded Quantum Dots*, Ph.D. thesis, Stanford University (2002).

[5] D. R. Stewart, *Level Spectroscopy of a Quantum Dot*, Ph.D. thesis, Stanford University (1999).

[6] H. van Houten *et al.*, Phys. Rev. B **39**, 8556 (1989).

[7] Yu. V. Sharvin, and N. I. Bogatina, Zh. Eksp. Teor. Fiz. **56**, 772 (1969).

[8] V. S. Tsoi, and I. I. Razgonov, Zh. Eksp. Teor. Fiz. **74**, 1137 (1978).

[9] G. Goldoni, and A. Fasolini, Phys. Rev. B **44**, 8369 (1991).

[10] K. Ohtsuka *et al.*, Phys. Rev. B **249**, 780 (1998).

[11] V. J. Goldman, B. Su, and J. K. Jain, Phys. Rev. Lett. **72**, 2065 (1994).

[12] L. W. Molenkamp *et al.*, Phys. Rev. B **41**, 1274 (1990).

[13] R. M. Potok *et al.*, Phys. Rev. Lett. **89**, 6602 (2002).

[14] J. A. Folk *et al.*, Science **299**, 679 (2003).

[15] B. J. van Wees *et al.*, Phys. Rev. Lett. **60**, 848 (1988).

[16] We have, including spin, $V_c = (I_{c\uparrow}+I_{c\downarrow})/g_c$, $I_{c\sigma} \propto I_{e\sigma}T_{c\sigma}$, and $g_c = (T_{c\uparrow}+T_{c\downarrow})(e^2/h)$, so $V_c \propto (I_{e\uparrow}T_{c\uparrow}+I_{e\downarrow}T_{c\downarrow})/(T_{c\uparrow}+T_{c\downarrow})$. H. Bruus, J. A. Folk, A. C. Johnson, and R. M. Potok (unpublished).

[17] K. J. Thomas *et al.*, Phys. Rev. Lett. **77**, 135 (1996).

[18] S. M. Cronenwett, *et al.*, Phys. Rev. Lett. **88**, 6805 (2002).

[19] D. H. Cobden *et al.*, Phys. Rev. Lett. **81**, 681 (1998).

[20] S. Luescher *et al.*, Phys. Rev. Lett. 86, 2114 (2001)

[21] S. Tans, M. H. Devoret, R. J. A. Groeneveld, and C. Dekker, Nature **394**, 761 (1998).

[22] D. R. Stewart *et al.*, Science **278**, 1784 (1997); D. Stewart, *Level Spectroscopy in Quantum Dots*, Ph.D. thesis, Stanford University (1998).

[23] U. Sivan *et al.* Phys. Rev. Lett. **77**, 1123 (1996); S. R. Patel *et al.*, Phys. Rev. Lett. **80**, 4522 (1998); F. Simmel *et al.* Phys. Rev. B **59**, 10441 (1999).

[24] L. P. Kouwenhoven *et al.*, Science **278**, 1788 (1997).

[25] P. W. Brouwer, Y. Oreg, and B. I. Halperin, Phys. Rev. B **60**, 13977 (2000); P. Jacquod and A. D. Stone, Phys. Rev. Lett. **84**, 3938 (2000); H. U. Baranger, D. Ullmo, L. I. Glazman, Phys. Rev. B **61**, R2425 (2000); I. L. Kurland, I. L. Aleiner, and B. L. Altshuler, cond-mat/0004205 (2000).

[26] D. C. Ralph, C. T. Black, and M. Tinkham, Phys. Rev. Lett. **78**, 4087 (1997).

[27] B. L. Altshuler, P. A. Lee, and R. Webb, eds., *Mesoscopic Phenomena in Solids* (North-Holland, Elsevier, 1991).

[28] C. W. J. Beenakker, Rev. Mod. Phys. **69**, 731 (1997).

[29] T. Guhr, A. Müller-Groeling, and H. A. Weidenmüller, Phys. Rept. **299**, 189 (1998).

[30] A. V. Khaetskii and Y. V. Nazarov, Phys. Rev. B **61**, 12639 (2000).

[31] B. I. Halperin *et al.*, Phys. Rev. Lett. **86**, 2106 (2001).

[32] I. L. Aleiner and V. I. Falko, Phys. Rev. Lett. **86**, 6801 (2001).

[33] D. M. Zumbuhl *et al.*, Phys. Rev. Lett. **89**, 6803 (2002).

[34] Y. B. Lyanda-Geller and A. D. Mirlin, Phys. Rev. Lett. **72**, 1894 (1994).

[35] B. L. Altshuler, and B. I. Shklovskii, Soviet Physics - JETP **64**, 127 (1986).

[36] J. S. Moon, N. O. Birge, and B. Golding, Phys. Rev. B **53**, R4193 (1996); J. S. Moon, N. O. Birge, and B. Golding, Phys. Rev. B **56**, 15124 (1997).

[37] P. Debray, J.-L. Pichard, J. Vicente, and P. N. Tung, Phys. Rev. Lett. **63**, 2264 (1989).

[38] I. H. Chan *et al.*, Phys. Rev. Lett. **74**, 3876 (1995).

[39] A. G. Huibers *et al.*, Phys. Rev. Lett. **81**, 1917 (1998).

[40] A. G. Huibers *et al.*, Phys. Rev. Lett. **81**, 200 (1998).

[41] H. U. Baranger and P. A. Mello, Phys. Rev. B **51**, 4703 (1995); P. W. Brouwer and C. W. J. Beenakker, Phys. Rev. B **51**, 7739 (1995); I. L. Aleiner and A. I. Larkin, Phys. Rev. B **54**, 14423 (1996); P. W. Brouwer and C. W. J. Beenakker, Phys. Rev. B **55**, 4695 (1997).

[42] R. M. Clarke *et al.*, Phys. Rev. B **52**, 2656 (1995).

[43] K. B. Efetov, Phys. Rev. Lett. **74**, 2299 (1995).

[44] *Semiconductor Spintronics and Quantum Computation*, eds. D. D. Awschalom, D. Loss, and N. Samarth, (Springer-Verlag, Germany, 2002).

[45] J. M. Kikkawa, and D. D. Awschalom, Phys. Rev. Lett. **80**, 4313 (1998).

[46] D. A. Wharam *et al.*, J. Phys. C **21**, L209 (1988).

[47] B. J. van Wees *et al.*, Phys. Rev. B **38**, 3625 (1988).

[48] F. J. Jedema *et al.*, Nature **416**, 713 (2002).

[49] P. R. Hammer and M. Johnson, Nature **8806**, 6806 (2002).

[50] R. Fiederling *et al.*, Nature **402**, 787 (1999).

[51] Y. Ohno *et al.*, Nature **402**, 790 (1999).

[52] C. W. J. Beenakker, Rev. Mod. Phys. **69**, 731 (1997).

[53] P. Brouwer, unpublished.

[54] P. Brouwer *et al.*, Phys. Rev. B **60**, 13977 (1999).

[55] P. Recher, E. V. Sukhorukov, and D. Loss, Phys. Rev. Lett. **85**, 1962 (2000).

[56] C. Gould *et al.*, Physica B **256**, 141 (1998).

[57] L. P. Kouwenhoven *et al.*, in *Mesoscopic Electron Transport*, edited by L. L. Sohn, L. P. Kouwenhoven, and G. Schön (Kluwer, Dordecht, 1997).